

ระเบียบวิธีปริมาตรจำกัดสำหรับการคาดคะเนการไหลแบบไม่ยุบตัวผ่านโดเมน
ที่มีขอบเขตโดยกำหนดความดันเป็นเงื่อนไขขอบ

นายดำรงศักดิ์ แย้มบางหวาย

วิทยานิพนธ์นี้เป็นส่วนหนึ่งของการศึกษาตามหลักสูตรปริญญาวิทยาศาสตรดุษฎีบัณฑิต
สาขาวิชาคณิตศาสตร์ประยุกต์
มหาวิทยาลัยเทคโนโลยีสุรนารี
ปีการศึกษา 2551

**FINITE VOLUME METHOD FOR THE
PREDICTION OF INCOMPRESSIBLE FLOW
THROUGH A BOUNDED DOMAIN WITH
SPECIFIED PRESSURE AS BOUNDARY
CONDITION**

Damrongsak Yambangwai

A Thesis Submitted in Partial Fulfillment of the Requirements for the
Degree of Doctor of Philosophy in Applied Mathematics
Suranaree University of Technology
Academic Year 2008

**FINITE VOLUME METHOD FOR THE PREDICTION OF
INCOMPRESSIBLE FLOW THROUGH A BOUNDED
DOMAIN WITH SPECIFIED PRESSURE AS
BOUNDARY CONDITION**

Suranaree University of Technology has approved this thesis submitted in partial fulfillment of the requirements for the Degree of Doctor of Philosophy.

Thesis Examining Committee

(Assoc. Prof. Dr. Prapasri Asawakun)

Chairperson

(Assoc. Prof. Dr. Nikolay Moshkin)

Member (Thesis Advisor)

(Prof. Dr. Sergey Meleshko)

Member

(Assoc. Prof. Dr. Ekachai Juntasaro)

Member

(Assoc. Prof. Dr. Varangrat Juntasaro)

Member

(Prof. Dr. Pairote Sattayatham)

Vice Rector for Academic Affairs

(Assoc. Prof. Dr. Prapan Manyum)

Dean of Institute of Science

ดำรงศักดิ์ เข้มบางหวาย : ระเบียบวิธีปริมาตรจำกัดสำหรับการคาดคะเนการไหลแบบไม่
ยุบตัวผ่านโดเมนที่มีขอบเขตโดยกำหนดความดันเป็นเงื่อนไขขอบ (FINITE
VOLUME METHOD FOR THE PREDICTION OF INCOMPRESSIBLE
FLOW THROUGH A BOUNDED DOMAIN WITH SPECIFIED
PRESSURE AS BOUNDARY CONDITION) อาจารย์ที่ปรึกษา :
รองศาสตราจารย์ ดร.นิโกลัน มอสกิน, 82 หน้า.

งานวิจัยนี้มีจุดประสงค์เพื่อนำเสนอปัญหาค่าขอบเริ่มต้นที่ดีในแบบต่างๆ ของปัญหา
เกี่ยวกับการไหลผ่านสำหรับสมการนาเวียร์-สโตกแบบไม่ยุบตัว ซึ่งเงื่อนไขขอบกำหนดด้วยความ
ดันหรือความดันรวม ในงานวิจัยนี้การแก้ปัญหาค่าขอบของการไหลผ่านของของไหลซึ่งอธิบายได้ด้วย
สมการนาเวียร์-สโตกแบบไม่ยุบตัวซึ่งมีผลเฉลยจริงที่เป็นไปได้เพียงหนึ่งเดียว ได้ถูกพัฒนาขึ้นโดย
ใช้ระเบียบวิธีปริมาตรจำกัดบนกริดที่สอดคล้องกับขอบแบบเฉียง อีกทั้งในงานวิจัยนี้ได้กล่าวถึง
การเตรียมเงื่อนไขขอบบริเวณที่ของไหลไหลผ่านเข้าและออก ผลที่ได้จากการคำนวณได้นำไป
เปรียบเทียบกับผลเฉลยเชิงวิเคราะห์ ข้อมูลจากการทดลองและผลเฉลยการคำนวณเชิงตัวเลขอื่นๆ
โดยพบว่าผลที่ได้เป็นที่น่าพอใจ

สาขาวิชาคณิตศาสตร์
ปีการศึกษา 2551

ลายมือชื่อนักศึกษา _____
ลายมือชื่ออาจารย์ที่ปรึกษา _____
ลายมือชื่ออาจารย์ที่ปรึกษาร่วม _____

DAMRONGSAK YAMBANGWAI : FINITE VOLUME METHOD FOR
THE PREDICTION OF INCOMPRESSIBLE FLOW THROUGH A
BOUNDED DOMAIN WITH SPECIFIED PRESSURE AS BOUNDARY
CONDITION. THESIS ADVISOR : ASSOC. PROF. NIKOLAY
MOSHKIN, Ph.D. 82 PP.

FINITE VOLUME METHOD/ INCOMPRESSIBLE FLUID/ FLOWING-
THROUGH/ BOUNDARY CONDITIONS.

The present study aims to present the overview of various kinds of well-posed flowing through initial boundary value problems for the incompressible Navier-Stokes equations with pressure or total pressure given on boundary. A finite volume method developed for solving a flowing through problem for the incompressible Navier-Stokes equations for which questions of existence and uniqueness have been proved. The computational method is based on the finite volume method in non-staggered boundary fitted grid. The implementation of boundary conditions on the through-flow parts (inlet and outlet) of boundary are discussed. The results of computations are compared with analytical solutions, experimental data and other numerical solutions and are found satisfactory.

School of Mathematics

Academic Year 2008

Student's Signature_____

Advisor's Signature_____

Co-advisor's Signature_____

ACKNOWLEDGEMENTS

I owe a debt of gratitude to the many people whose encouragement, assistance, and support have enabled me to complete this research project.

First, I wish to express my deep gratitude to Assoc. Prof. Dr. Nikolay Moshkin, my thesis advisor, for his encouragement, advice, and guidance. I was fortunate to have an opportunity to work with him. My gratitude is also extend to Prof. Dr. Christo Christov, my thesis co-advisor, for his kind assistance in editing, proof reading, and giving fruitful advice.

I would like to acknowledge the personal and professional support received from the faculty of the School of Mathematics, Suranaree University of Technology: Assoc. Prof. Dr. Prapasri Asawakun, Prof. Dr.Pairote Sattayatham, Prof. Dr. Sergey Meleshko, Asst. Prof. Dr. Eckart Schulz, and Asst. Prof. Dr. Arjuna Peter Chaiyasena.

Thank also to my dissertation committee members, Assoc. Prof. Dr. Prapasri Asawakun, Prof. Dr. Sergey Meleshko, Prof. Dr. Ekachai Juntasaro, and Assoc. Prof. Dr. Varangrat Juntasaro, who gave me useful suggestion.

I wish to thank all my friends at Suranaree University of Technology for their friendly help. I would like to thank Dr. Chittima Kaweera, who were always there for me and helped me get through a very though time completing this research project.

I am also indebted to The Royal Golden Jubilee Ph.D Program (RGJ) and The Development and Promotion of Science and Technology Talents Project (DPST) for providing a full scholarship to study in Thailand.

Finally, I wish to dedicate this research to my parents and my sister. Without their continuous love and support, I would not have been to complete my study.

Damrongsak Yambangwai

CONTENTS

	Page
ABSTRACT IN THAI	I
ABSTRACT IN ENGLISH	II
ACKNOWLEDGEMENTS	III
CONTENTS	IV
LIST OF TABLES	VI
LIST OF FIGURES	VII
 CHAPTER	
I INTRODUCTION	1
1.1 Objective and overview	1
1.2 Finite volume method	4
1.3 A two-dimensional interpolation function for irregularly space data	6
1.4 Technics to estimate the order of convergence	8
II MATHEMATICAL MODELS OF FLOWING THROUGH PROBLEM	9
2.1 Well-posed flowing through problem	9
2.2 Example of flowing through problems	11
2.2.1 Flow in a pipe joining two plenums at different pressure	11
2.2.2 Flow through branching channels	12
2.2.3 Ventilation in buildings	14
III NUMERICAL ALGORITHMS AND VALIDATION TESTS	15
3.1 Discretizations	15
3.2 Validation Test	26

CONTENTS (Continued)

	Page
3.2.1 Flow between two parallel plates	26
3.2.2 Flow with Circular Streamline	28
IV FLOW IN PLANAR T-JUNCTION CHANNEL	33
4.1 Validation tests	36
4.2 Flow driven by pressure differences in a 90° planar T-junctions	47
V FLOW IN U-BEND CHANNEL	58
5.1 Steady flow in U-bend channel	58
5.2 Oscillating flow through U-bend channel	62
VI GENERAL SUMMARY AND CONCLUSIONS	69
6.1 General summary and conclusions	69
6.2 Contribution to knowledge	70
6.3 Recommendation for future research	71
REFERENCES	73
APPENDICES	
APPENDIX A EXACT SOLUTIONS	78
A.1 Analytical solution of steady flow between two parallel plates	78
A.2 Analytical solution of oscillating flow between two parallel plates	80
CURRICULUM VITAE	82

LIST OF TABLES

Table		Page
3.1	Test cases $0 \leq \theta \leq \pi$, $\vec{u} = (u_x, u_y)$, and $H(r) = p + \frac{1}{2}u_y^2$	31
3.2	Rate of convergence. Four test cases, $K = 500$	31
4.1	Flow split, $Re = 10, 100, 200, 300, 400$	40
4.2	Flow split in upper branch for $Re_Q = 248$ and $p_3 = 0.129$	44
4.3	X_R and Y_R for $Re_Q = 248$ and $\beta = 0.44$	45
4.4	X_R and Y_R for $Re_Q = 248$	47
5.1	Darcy friction for three kinds of the flowing through problem, $Re = 100, \delta = 3$	61

LIST OF FIGURES

Figure		Page
1.1	Types of Finite volume grids, nodes centered in control volume (left), and control volume faces centered between nodes (right).	5
1.2	Data points.	7
2.1	Sketch of the flowing through domain	10
2.2	Flow in a pipe joining two plenums at different pressures.	12
2.3	Flow through branching channel.	13
3.1	A typical 2D control volume with the notation used and a way of calculating cell face value and gradients.	17
3.2	Sketch of the problem. Flow between two parallel plates.	27
3.3	The relation between Re_Q and $Re_{\Delta p}$	28
3.4	Volume rate vs time, $Re_{\Delta p} = 150$	28
3.5	Sketch of problem domain. Circular streamline.	29
3.6	Velocity profile at the vertical line $\theta = \pi/2$ (component u_x) for the Case 1 and different values of K	32
3.7	Pressure along the line $\theta = \pi/2$, $K = 500$ for Case 1.	32
4.1	Schematic geometry of T-junction bifurcation and coordinate system.	36
4.2	The flow rate ratio, β^* , as a function of Reynolds number, Re	39
4.3	Streamline patterns and pressure contour of flow in the T-junction for various Re , and equal static pressure at the exists Γ_2^1 and Γ_3^1	41
4.4	The relation between p_3 and β for $Re_Q = 248$	42
4.5	Comparison between experimental data of Liepsch <i>et al.</i> (1982) and numerical data of Miranda <i>et al.</i> (2008) ($Re_Q = 248$ and $\beta = 0.44$)	43

LIST OF FIGURES (Continued)

Figure		Page
4.6	Developing of Main and secondary recirculation zone as a function of flow split β	46
4.7	Diagram of flow regime.	49
4.8	The streamline (left column) and pressure contours (right column) for impacting T-junction. See cross signs (\times) on line OG in Figure 4.7. .	53
4.9	The streamline (left column) and pressure contours (right column) for the case correspond to triangle signs (Δ) on line OC in Figure 4.7. .	54
4.10	The streamline (left column) and pressure contours (right column) for the case correspond to square signs (\square) on line OF in Figure 4.7. . .	55
4.11	The streamline (left column) and pressure contours (right column) for the case correspond to down triangle signs (∇) on line OD in Figure 4.7.	56
4.12	The streamline (left column) and pressure contours (right column) for the case correspond to circle signs (\bigcirc) on line OB in Figure 4.7. . .	57
5.1	Schematic diagram of U-bend channel.	59
5.2	Friction factor as a function of Reynolds number.	62
5.3	Streamline patterns of flow in the U-bend channel for various δ and Re .	63
5.4	Schematic diagram of oscillating flow in U-bend channel.	64
5.5	Predicted variation of volume rate with time.	66
5.6	Schematic diagram of damped oscillatory motion regime.	66
5.7	Variations of volume rate with time. Influence of initial displacement.	67
5.8	Variation of volume rate with time. Influence of Fr	67
5.9	Variation of volume rate with time. Influence of curvature ratio δ . . .	67
5.10	Period of oscillation with Fr	67
A.1	Sketch of problem domain	78

CHAPTER I

INTRODUCTION

1.1 Objective and overview

A flow of an viscous incompressible fluid through a given domain is rather interesting for its numerous engineering applications. Typically, these include tube and channel flows with a variety of geometries. The difficulties in mathematical modelling and numerical simulation of such flows rise in the through-flow boundaries (inflow and outflow). If the domain of interest is completely bounded by impermeable walls, there is no ambiguity in the boundary conditions for incompressible Navier-Stokes equations. However, when through-flow (inflow and outflow) boundaries are present, there is no general agreement on which kind of boundary conditions are both mathematically correct and physically appropriate on these through-flow boundaries. Traditionally, such problems are treated with specified velocity on the domain boundaries. However, in many applications the boundary velocities are not known, instead the pressure variation is given at the boundaries and the flow within domain has to be determined. For example, in the central air-conditioning or air-heating system of a building, a main supply channel branches into many sub-channels that finally open into the different rooms, which can be at a different constant pressure. The distribution of the flow into various branches depends on the flow resistances of these branches and in a general case, it is even impossible to predict the direction of flow.

The problem of solvability and uniqueness of initial boundary value problem for the incompressible Navier-Stokes equations is one of the various problems considered for example in Antontsev *et al.* (1990), Ladyzenskaya (1963), Ragulin (1976),

Ragulin *et al.* (1980), Temam (1981) and many others. Antontsev *et al.* (1990), Ragulin (1976), and Ragulin *et al.* (1980) have studied initial boundary value problems in which the values of pressure or total pressure are specified on through-flow boundaries. Ragulin (1976) and Ragulin *et al.* (1980) have considered problem for homogeneous Navier-Stokes equations. Antontsev *et al.* (1990) has studied well-posedness of nonhomogeneous Navier-Stokes equations. As these results are not well known, we shall shortly represent the well-posed statement of initial boundary value problems with specified pressure boundaries.

To the best of the authors knowledge, the research on numerically treated pressure boundary conditions for the incompressible Navier-Stokes equations is limited. Some of the research conducted is discussed below. Kuznetsov *et al.* (1983) and Moshkin (1983, 1985, 1986) developed finite difference algorithms to treat incompressible viscous flow in domain with given pressure on through-flow parts of the boundary. Finite difference numerical algorithms were developed for primitive variables and for stream function vorticity formulation of 2D Navier-stokes equations.

In the finite-element study by Hayes *et al.* (1989), a brief discussion of the specified pressure on the outflow region of the boundary is presented. Kobayashi *et al.* (1993) have discussed the role of pressure specified on open boundaries in the context of the SIMPLE algorithm.

The prescription of a pressure drop between the inlet at the outlet of the flow was also considered by Heywood *et al.* (1996), where a variational approach with given mean values of the pressure across the inflow and outflow boundaries was used.

The construction of the discretized equations for unknown velocities on specified pressure boundaries and the solution of the discretized equations using the SIMPLE algorithm are discussed in Kelkar and Choudhury (2000). The computational treatment of specified pressure boundaries in complex geometries is presented within the framework of a non-staggered technique based on curvilinear boundary-fitted

grids. The proposed method is applied for predicting incompressible forced flows in branched ducts and in buoyancy-driven flows.

A finite-difference method for solving the incompressible time-dependent three-dimensional NavierStokes equations in open flows where Dirichlet boundary conditions for the pressure are given on part of the boundary is presented in Fernandez and Sanmiguel (2004). The equations in primitive variables (velocity and pressure) are solved using a projection method on a non-staggered grid with second-order accuracy in space and time. On the inflow and outflow boundaries the pressure is obtained from its given value at the contour of these surfaces using a two dimensional form of the pressure Poisson equation, which enforces the incompressibility constraint $\nabla \cdot v = 0$. The pressure obtained on these surfaces is used as Dirichlet boundary conditions for the three-dimensional Poisson equation inside the domain. The solenoidal requirement imposes some restrictions on the choice of the open surfaces.

William and Graham (2007) discussed the choice of appropriate inflow and outflow boundary conditions for Newtonian and generalized Newtonian channel flows. They came to conclusion, that “...*For real-world problems that are fundamentally pressure driven and involve complex geometries, it is desirable to impose a pressure drop by means of specified pressures at the inflow and outflow boundaries...*”. At the inflow and outflow boundaries one of the condition specifies the normal component of the surface traction force, and the other two imply there is no tangential flow at these boundaries; that is, flow is normal to the inflow and outflow boundaries. But no mathematical justification was given.

Let us called problems where fluid can enter or leave domain through parts of boundary as “*flowing through problem*” for viscous incompressible fluid flow. In Fernandez and Sanmiguel (2004) these problems are called problems with “*open*” boundaries. We think the term “*flowing through problem*” is more suitable. The

purpose of our research is not to add new insight into the mathematical statement of the problem, but to develop a finite volume method for solving a flowing through problem for the incompressible Navier-Stokes equations for which questions of existence and uniqueness have been considered in Antontsev *et al.* (1990), Ragulin (1976), and Ragulin *et al.* (1980).

A brief overview of various kinds of well-posed flowing through initial boundary value problems for the incompressible Navier-Stokes equations is presented in Chapter II. This is followed by description of the finite volume numerical method with strength on the implementation of boundary conditions on the through-flow parts. The numerical method is then validated by comparison analytical and numerical solutions for the laminar flow driven by pressure drop in the two-dimensional plane channel and the two-dimensional gap between two cylinders in Chapter III. In Chapter IV, the numerical method is then validated by comparing our numerical results with known experimental and computational data for the two dimensional laminar flow through a 90° T-junction channel. The computed solutions are analyzed in terms of flow topology patterns depending on pressure drop between T-junction branches. In Chapter V, the two-dimensional steady flow and oscillating flow of an incompressible viscous fluid in U-bend channel is considered.

1.2 Finite volume method

Conservation laws can be derived by considering a given quantity of matter and its extensive properties, such as mass, momentum, and energy. In fluid flows, however, it is difficult to follow a parcel of matter. It is more convenient to deal with the flow within a certain spatial region, we call control volume Ω . We consider only the generic conservation equation for a quantity ϕ and assume that the velocity field and all fluid properties are known. The finite volume method uses the integral form

of conservation equation as the starting point:

$$\frac{\partial}{\partial t} \int_{\Omega} \rho \phi \, d\Omega + \oint_S \rho \phi \vec{u} \cdot \vec{n} \, dS = \oint_S \Gamma \nabla \phi \cdot \vec{n} \, ds + \int_{\Omega} q_{\phi} \cdot \vec{n} \, d\Omega, \quad (1.1)$$

where S is the boundary of control volume Ω , \vec{n} is the unit outward normal vector to S , \vec{u} is velocity field, Γ is the diffusivity for the quantity ϕ , and q_{ϕ} is the source or sink of ϕ .

The solution domain is subdivided into a finite number of small control volumes by a grid which, in contrast to the finite difference method, define the control volume boundaries, not the computational nodes. The usual approach is to define control volume by a suitable grid and assign computational node to the control volume center (see Figure 1.1 a)). However, one could as well (for structure grids) define the nodal locations first and construct control volumes around them, so that control volume faces lies midway between nodes (see Figure 1.1 b)). Nodes on which boundary conditions are applied are shown as full symbols in this figure. The advantage of the second approach is the linear approximations between two nearest nodes of derivative at control volume faces are more accurate when the face is midway between two nodes. The advantage for the first approach is that the nodal value represents

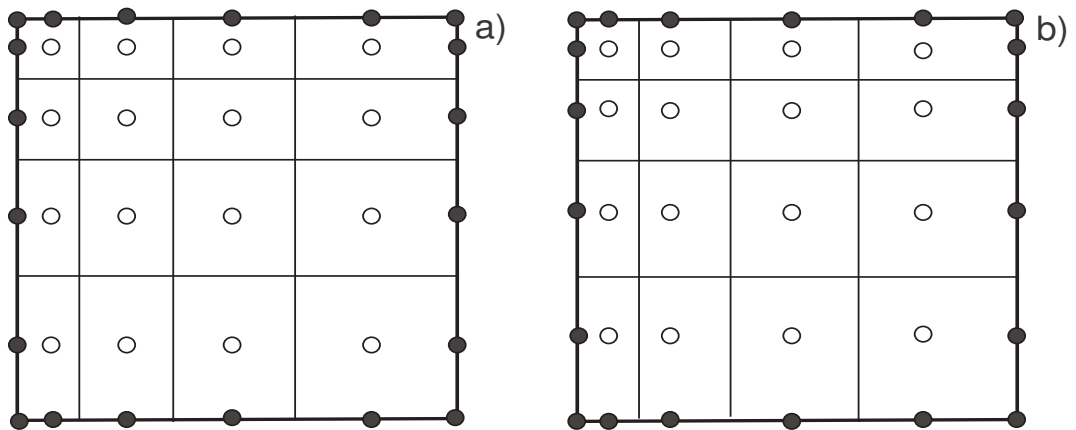


Figure 1.1 Types of Finite volume grids, nodes centered in control volume (left), and control volume faces centered between nodes (right).

the mean over the volume of control volume to higher accuracy (second order) than

in the first approach, since the node is located at the centroid of the control volume. The first variant is used more often and will be adopted in this research.

The integral conservation equation (1.1) applies to each control volume, as well as to the solution domain as a whole. If we sum equations for all control volume, we obtain the global conservation equation, since surface integrals over the inner control volume faces cancel out. Thus global conservation is built into the method and this provides one of the principle advantage. To obtain an algebraic equation for particular control volume, the surface and volume integrals need be approximates.

1.3 A two-dimensional interpolation function for irregularly space data

A problem that often arises in data analysis is interpolation, that is, estimating the value of a function between points at which the function is known. On this research, there arises a need for the two-dimensional interpolating from irregularly spaced data. The two-dimensional interpolation takes a series of (x_i, y_i, z_i) , $i = 1, \dots, N$ points and generates estimated values for z at new (x, y) points. The way of interpolation on this research is the two-dimensional interpolation based on a weighted average of the value at the data point in Donald, (1968). The weighting was a function of distance to those points, would satisfy the criteria (function is continuously differentiable). It is assume that a finite number N of triplets (x_i, y_i, z_i) are given, where x_i, y_i are the locational coordinates of the data point D_i , and z_i is the corresponding data value. Data point location may not be coincident. An interpolation function $z = f(x, y)$ to assign a value to any location $P(x, y)$ in the plane is sought. Two-dimensional interpolation is to be smooth (continuous and once differentiable), to pass through the specified points, (i.e., $f(x_i, y_i) = z_i$), and to meet the user's intuitive expectation about the phenomenon under investigation.

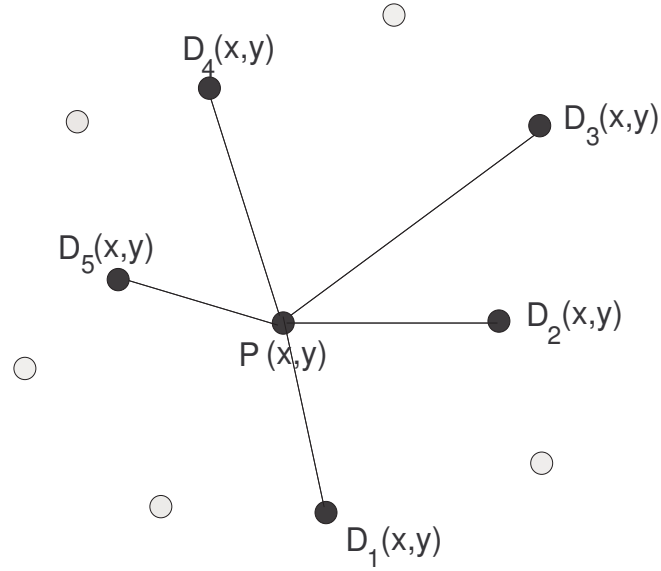


Figure 1.2 Data points.

Furthermore, the function should be suitable for computer application at reasonable cost. Using the coordinates $P(x, y)$ and $D_i(x, y)$, z_i be the value at the data point D_i , and $L_{(P,D_i)}$ be the Cartesian distance between P and D_i . The interpolated value at P is

$$f(P) = \begin{bmatrix} \frac{\sum_i L_{(P,D_i)}^{-2} z_i}{\sum_i L_{(P,D_i)}^{-2}} & \text{if } L_{(P,D_i)} \neq 0 \text{ for all } D_i \\ z_i & \text{if } L_{(P,D_i)} = 0 \text{ for all } D_i \end{bmatrix}, \quad (1.2)$$

where $L_{(P,D_i)}^{-2} = 1/[(x_P - x_{D_i})^2 + (y_P - y_{D_i})^2]$. Notice that as P approach a data point D_i , $L_{(P,D_i)} \rightarrow 0$, and the i^{th} terms in the numerator and denominator exceed all bounds while the other terms remains bounded. Therefore $\lim_{P \rightarrow D_i} f(P) = z_i$ as desired, and the function $f(P)$ is continuous.

1.4 Technics to estimate the order of convergence

To evaluate rate of convergence on spatial variables the solution was obtained on a sequence of grids. To estimate the rate of convergence, the validity of expression

$$f_{ex} \approx f_{ap} + Ch^\alpha, \quad (1.3)$$

is accepted where f_{ex} and f_{ap} are quantities related to an exact and approximated solution, respectively. Parameters C , α , and h are the error constant, the rate of convergence, and mesh size respectively. Coefficients C and α independent of h . To compute the rate of convergence, the following step is applied. Let Ω^h be discrete domain, f_{ex}^h be a projection of exact solution of the differential problem on a set of grid function given on Ω^h , f_{ap}^h is a solution of a finite difference scheme on a mesh Ω^h , and $h \in R^h$ where R^h is the range of h in which numerical solution can be computed. Choose any convenient value h_1 such that $h_1, h_1/m \in R^h$. The first step is to use the numerical method to compute the two numerical solutions of the problem for two grids Ω_{h_1} and $\Omega_{h_1/m}$ respectively. The second step is to compute the norm of difference between between f_{ex}^h and f_{ap}^h on grid Ω_{h_1} and $\Omega_{h_1/m}$.

$$D_1 = \|f_{ex}^{h_1} - f_{ap}^{h_1}\|_{\Omega_{h_1}} \approx Ch_1^\alpha, \quad D_2 = \|f_{ex}^{h_1/m} - f_{ap}^{h_1/m}\|_{\Omega_{h_1/m}} \approx C \left(\frac{h_1}{m}\right)^\alpha. \quad (1.4)$$

Dividing D_1 by D_2 , we obtained

$$\frac{D_1}{D_2} \approx m^\alpha. \quad (1.5)$$

Taking the natural logarithm on both sides, we get an approximate value for the rate of convergence

$$\alpha \approx \frac{\ln\left(\frac{D_1}{D_2}\right)}{\ln m}. \quad (1.6)$$

Usually in practice m is equal 2. In case where exact solution is unknown, we need to perform computations at least on three refined grids. Solution on finest grid excepted as exact solution and rate of convergence estimated by (1.4)-(1.6).

CHAPTER II

MATHEMATICAL MODELS OF FLOWING THROUGH PROBLEM

In this chapter, various kinds of well-posed flowing through problems for the incompressible Navier-Stokes equations and the particular examples of flowing through problem are presented.

2.1 Well-posed flowing through problem

We present here the various kinds of well-posed flowing through boundary value problems for the incompressible Navier-Stokes equation. In our explanation we follow Antontsev *et al.* (1990), Ragulin (1976), and Ragulin *et al.* (1980). Let us consider the flow of viscous liquid through bounded domain Q of R^3 . Let Γ_k^1 , $k = 1, \dots, K$ denote parts of the boundary $\Gamma = \partial Q$ where the fluid enter or leave the domain. Let Γ_l^0 , $l = 1, \dots, L$ be an impermeable parts of the boundary, $D = Q \times (0, T)$, $S = \Gamma \times (0, T)$, $S^\alpha = \Gamma^\alpha \times (0, T)$, $\alpha = 0, 1$. Scheme of the domain is depicted in Figure 2.1. The flowing through problem is to find a solution of the Navier-Stokes system

$$\frac{\partial \vec{u}}{\partial t} + (\vec{u} \cdot \nabla) \vec{u} = -\frac{1}{\rho} \nabla p + \nu \Delta \vec{u}, \quad (2.1)$$

$$\nabla \cdot \vec{u} = 0, \quad (2.2)$$

in the domain $D = Q \times (0, T)$ with appropriate initial and boundary conditions, where \vec{u} is the velocity vector, p is the pressure, ρ is the density, and ν is the kinematics viscosity. The initial data are

$$\vec{u} |_{t=0} = \vec{u}^0(\vec{x}), \quad \nabla \cdot \vec{u}^0 = 0, \quad \vec{x} \in Q. \quad (2.3)$$

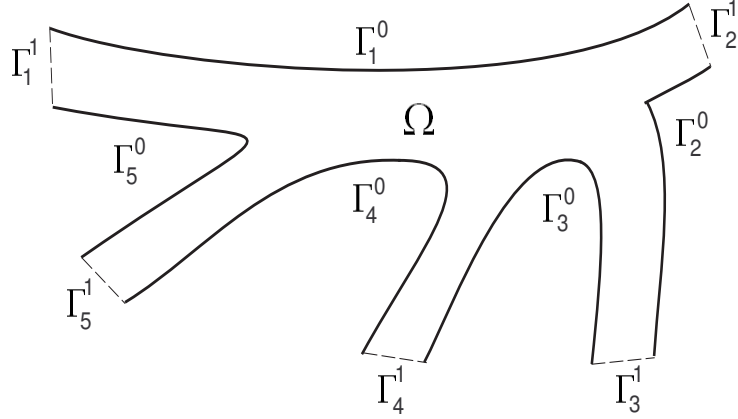


Figure 2.1 Sketch of the flowing through domain

On the solid wall Γ_l^0 , the no-slip condition holds

$$\vec{u} = 0, (\vec{x}, t) \in S_l^0, l = 1, \dots, L. \quad (2.4)$$

On through-flow parts Γ_k^1 , $k = 1, \dots, K$, three types of boundary conditions can be set up to make problem well-posed. As shown in Antontsev *et al.* (1990), Ragulin, (1976) the conditions are the following:

- On the through-flow parts Γ_j^1 , $j = j_1, \dots, j_n$, the tangent components of the velocity vector and the total pressure are prescribed

$$\begin{aligned} \vec{u} \cdot \vec{\tau}_m &= G_j^m(\vec{x}, t), m = 1, 2, \\ p + \frac{1}{2}\rho|\vec{u}^2| &= H_j(\vec{x}, t), (\vec{x}, t) \in S_j^1, j = j_1, \dots, j_n. \end{aligned} \quad (2.5)$$

Here $\vec{\tau}_1, \vec{\tau}_2$ are the linearly independent vectors tangent to Γ_j^1 . Functions $G_j^m(\vec{x}, t)$, and $H_j(\vec{x}, t)$ are given on $S_j^1 = \Gamma_j^1 \times (0, T)$.

- On the through-flow parts Γ_l^1 , $l = l_1, \dots, l_n$, the tangent components of the velocity vector and pressure are known

$$\begin{aligned} \vec{u} \cdot \vec{\tau}_m &= G_l^m(\vec{x}, t), m = 1, 2, \\ p &= H_l(\vec{x}, t), (\vec{x}, t) \in S_l^1, l = l_1, \dots, l_n. \end{aligned} \quad (2.6)$$

Here $G_l^m(\vec{x}, t)$, and $H_l(\vec{x}, t)$ are given on $S_l^1 = \Gamma_l^1 \times (0, T)$.

- On the through-flow parts Γ_s^1 , $s = s_1, \dots, s_n$, the velocity vector (all three components) has to be prescribed

$$\vec{u} = \vec{u}_s^1(\vec{x}, t), (\vec{x}, t) \in S_s^1, s = s_1, \dots, s_n. \quad (2.7)$$

Here $\vec{u}_s^1(\vec{x}, t)$ is given on $S_s^1 = \Gamma_s^1 \times (0, T)$.

It should be mentioned that various combination of boundary conditions on S_k^1 , $k = 1, \dots, K$ give the well-posed problems. For example, on the portion of the through-flow parts S_j^1 , $j = j_1, \dots, j_n$ one kind of boundary condition may hold and on other portions another kinds may hold.

2.2 Example of flowing through problems

The example of the flowing through problems are the flow in a pipe joining two plenums, the flow through branching channels, blood flow in veins and arteries in human bodies, and many others.

2.2.1 Flow in a pipe joining two plenums at different pressure

Kelkar and Choudhury (2000) consider the physical plenums shown in Figure 2.2 for motivating the mathematical description of the specified pressure boundaries. The physical situation consists of a pipe connected to two reservoirs. When the pressure in the left plenum, p_L , is higher than the pressure in the right reservoir, p_R , a flow occurs through the pipe from left to right. The flow issuing from the tube into the right plenum behaves like a free jet, and it dissipates its kinetic energy due to viscous action. Thus, the static pressure over the exit cross section of the tube is very close to the chamber pressure p_R . However, in the left plenum, the flow accelerates from the plenum pressure p_L to a lower static pressure at the inlet of the

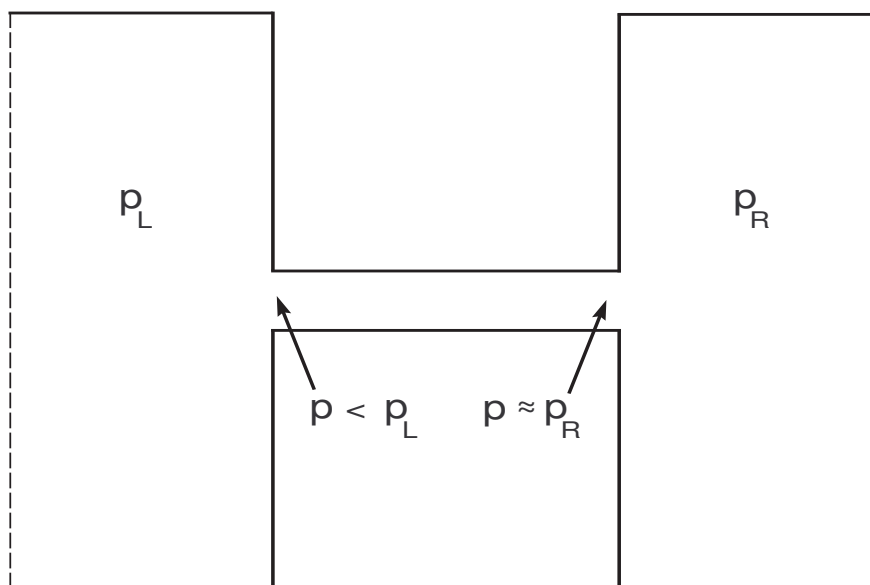


Figure 2.2 Flow in a pipe joining two plenums at different pressures.

tube. This decrease in pressure at the inlet cross section from its value in the plenum is dependent on the flow velocity and is not known a priori. Further, the flow in the plenum can be assumed to be inviscid so the Bernoulli equation can be applied to relate the static pressure and the velocity head at the tube inlet to the plenum pressure. The plenum pressure is thus the stagnation pressure for the inflow. It is clear from the above discussion that the interpretation of the specified pressure on a domain boundary is dependent on the direction of the flow at the domain boundary. If the pipe is taken to be the computational domain, the specified pressure is the stagnation pressure if the flow enters the domain, while it is the static pressure if the flow leaves the domain. A complete specification of the flow conditions at a specified pressure boundary also needs knowledge of the flow direction.

2.2.2 Flow through branching channels

The flow through branching channels has been used in industrial application, such as piping systems and ventilation system. For example, in the air-conditioning system of an automobile, a main supply duct branches into many ducts that open

into the passenger compartment which is at constant pressure (see Kelkar and Choudhury, 2000). There are three types of boundary conditions relevant to the flow

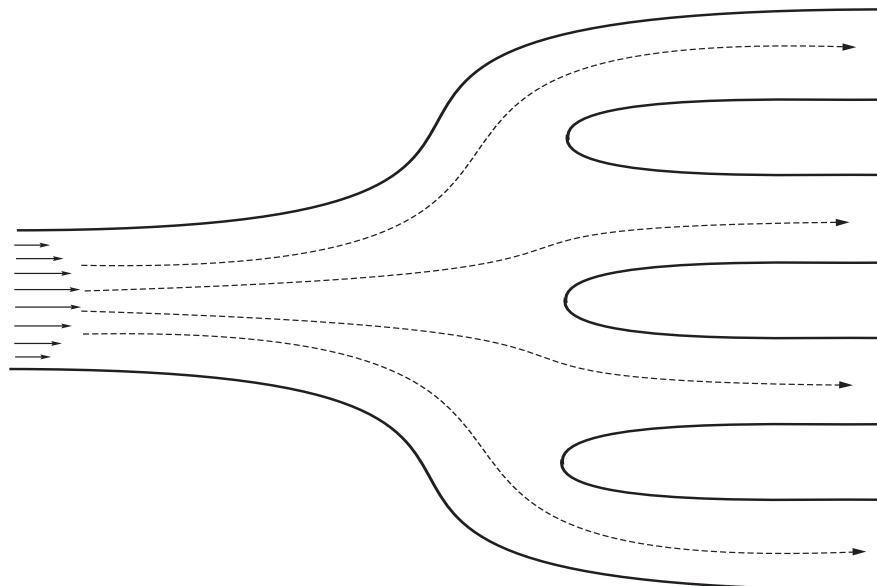


Figure 2.3 Flow through branching channel.

through branching channels: inlets, outlets, and solid wall. For example, at the inlet, the stream wise velocity component and the shear stress component are prescribed. Typically, the velocity follows a parabolic shape for the steady flow. At the wall the no-slip condition is applied directly. Finally on the outlet parts, one can either prescribed the pressure or total pressure. The pattern of flow, the separation flow rate, and the recirculating zone when the fluid passes the branch junction (see Figure 2.3), are investigated and shown in many article.

The flow through branching channels is encountered in human bodies. The vascular system depends on the branches to distribute blood. The arterial walls in the branching regions are exposed to high and low shear stress which disturb local mass transfer and cause cell degradation. In living organisms bifurcating flows have characteristics of their own, such as flow unsteadiness, pulsating flow regime due to variable pressure gradient, non-linear rheology, specific flow geometry.

2.2.3 Ventilation in buildings

Others example of pressure driven flow is the study of indoor environmental quality. Study of indoor air quality needs information of airflow in buildings. Computational Fluid Dynamics (CFD) can give a detailed distribution of airflow and contaminant concentration for a building. It is straightforward to specify mass flow rates as boundary condition in a CFD code. Pressure boundary condition usually receives more attention in the context of compressible flows. For incompressible flows (such as flow in buildings), a pressure condition is not need at a boundary if velocities can be specified because they are interested. This works well for mechanically ventilated buildings where flow rate from air supply diffusers are known and flow direction can be predetermined. However, for many other types of flow in a building, pressure at boundary can be determined but not the velocities. A typical example is nature ventilation in a building where pressure at open windows are known but the ventilation rate needs to be determined. Hence, to be able to specify pressure boundary conditions in a CFD program is important. Very few studies of pressure boundary condition are available for incompressible flow.

CHAPTER III

NUMERICAL ALGORITHMS AND VALIDATION TESTS

In this chapter, we present numerical algorithms for the solution of the flowing through problems in which the governing equations are incompressible Navier-Stokes equation. The numerical methods are developed for fluid flow through domain with the combination of three kinds of boundary conditions specified on the through-flow parts (inlet and outlet). To demonstrate the efficiency of our numerical algorithms, we give the examples of flow between two parallel plates and flow with circular streamline for which the analytical solutions are known.

3.1 Discretizations

Let us present the numerical algorithm for flowing through problem. Although some of the main aspects are well known in the literature, for the sake of completeness the issue is illustrated. The time discretization used here is based upon variation of the projection scheme originally proposed by Chorin and Marsden (1968). Using the explicit Euler time stepping, the marching steps in the time are the following Set $\vec{u} |_{t=0} = \vec{u}^0$, then for $n \geq 0$ compute \vec{u}^* , \vec{u}^{n+1} , and p^{n+1} by solving

First sub-step:

$$\frac{\vec{u}^* - \vec{u}^n}{\Delta t} + (\vec{u}^n \cdot \nabla) \vec{u}^n = \nu \Delta \vec{u}^n. \quad (3.1)$$

Second sub-step:

$$\frac{\vec{u}^{n+1} - \vec{u}^*}{\Delta t} = -\nabla p^{n+1}, \quad (3.2)$$

$$\nabla \cdot \vec{u}^{n+1} = 0, \quad (\vec{u}^{n+1})_{\Gamma^0} = 0, \quad (3.3)$$

where $\Delta t = T/N$ is the time step, N is the integer, $\vec{u}^n \approx \vec{u}(\vec{x}, n\Delta t)$, and $p^{n+1} \approx p(\vec{x}, (n+1)\Delta t)$. Without loss of generality density is equal to one, $\rho = 1$.

For the sake of simplicity and without losing generality, the formulation of numerical algorithm is illustrated for a two-dimensional domain. Let $\vec{u} = (u_x, u_y)$ be velocity vector, where u_x and u_y are the Cartesian components in x and y direction, respectively. The finite volume discretization is represented for non-orthogonal quadrilaterals grid. The collocated variable arrangement is utilized. Each discrete unknown is associated with center of control volume Ω . First, we discretize the convection and diffusion part of the Navier-Stokes equation. One can recast equation (3.1) in the form

$$\frac{\phi^* - \phi^n}{\Delta t} + \nabla \cdot (\phi^n \vec{u}^n) = \nu \Delta \phi^n, \quad (3.4)$$

where the variable ϕ can be either u_x or u_y and \vec{u}^n is such that $\nabla \cdot \vec{u}^n = 0$. The discrete form of (3.4) is obtained by integrating on each control volume Ω , followed by the application of the Gauss theorem:

$$\int_{\Omega} \frac{\phi^* - \phi^n}{\Delta t} d\Omega + \oint_S \phi^n (\vec{u}^n \cdot \vec{n}) dS = \nu \oint_S \nabla \phi^n \cdot \vec{n} dS, \quad (3.5)$$

where S is the boundary of control volume Ω (for example, in the case shown in Figure 3.1, S is the union of the control volume faces s, e, n, w) and \vec{n} is the unit outward normal vector to S . Using the midpoint rule to approximation the surface and volume integrals yields

$$\int_{\Omega} \frac{\phi^* - \phi^n}{\Delta t} d\Omega \approx \left(\frac{\phi^* - \phi^n}{\Delta t} \right)_P \Delta \Omega, \quad (3.6)$$

$$\oint_S \phi^n (\vec{u}^n \cdot \vec{n}) dS \approx \sum_{c=e,s,n,w} \phi_c^n (\vec{u}^n \cdot \vec{n})_c S_c, \quad (3.7)$$

$$\oint_S \nabla \phi^n \cdot \vec{n} dS = \oint_S D_n \phi^n dS \approx \sum_{c=e,s,n,w} (D_n \phi^n)_c S_c, \quad (3.8)$$

where $\Delta \Omega$ is the volume of control volume Ω , S_c is the area of the “ c ” control volume face, and $(D_n \phi)_c$ is the derivative of Cartesian velocity components in the normal

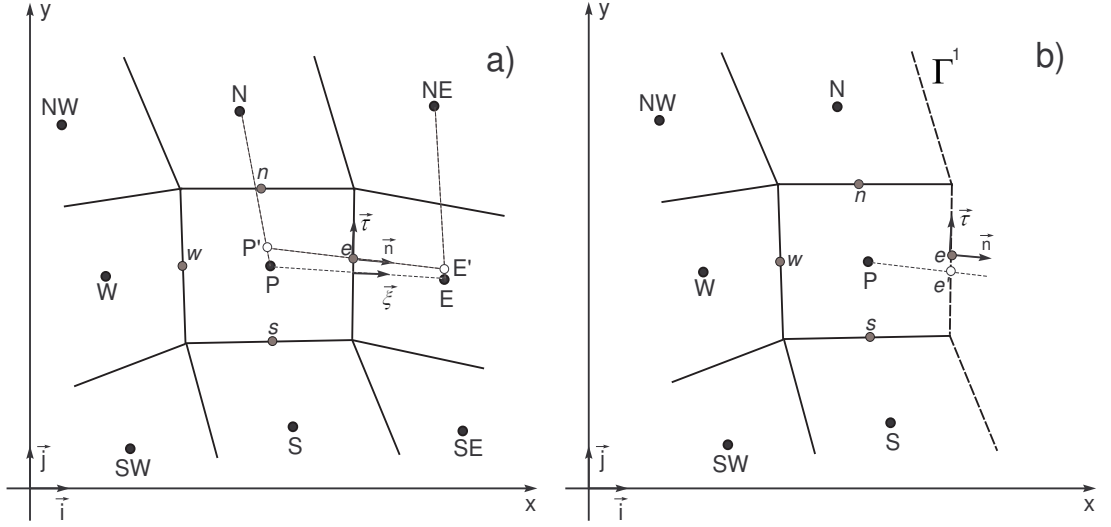


Figure 3.1 A typical 2D control volume with the notation used and a way of calculating cell face value and gradients.

direction at the center of the “c” control volume face. To estimate the right hand side in equations (3.7) and (3.8), we need to know the value of Cartesian velocity components and its normal derivative on the faces of each control volume. The implementation of Cartesian velocity components on non-orthogonal grids requires special attention because the boundary of the control volume is usually not aligned with the Cartesian velocity components. The 2D interpolation of irregularly-spaced data (see for example Donald, 1968) is used to interpolate Cartesian velocity components on the boundary of each control volume in equation (3.7). Only the east side of a 2D control volume shown in Figure 3.1 a) will be considered. The same approach applies to other faces, only the indices need to be changed. For example, let ϕ_k be the value of Cartesian velocity component at point k where $k = N, P, S, SE, E, NE$ and $L_{(e,k)}$ be the Cartesian distance between e and k . Using 2D interpolation yields

$$\phi_e = \left(\sum_k L_{(e,k)}^{-2} \phi_k \right) / \left(\sum_k L_{(e,k)}^{-2} \right), \quad k = N, P, S, SE, E, NE, \quad (3.9)$$

where $L_{(e,k)}^{-2} = 1/[(x_e - x_k)^2 + (y_e - y_k)^2]$.

The derivative of Cartesian velocity components in the normal direction at

the center of the control volume face in equation (3.8) can be calculated by using the central difference approximation (see Figure 3.1 a))

$$(D_n\phi)_e \approx \frac{\phi_{E'} - \phi_{P'}}{L_{(P',E')}}.$$

The auxiliary nodes P' and E' lie at the intersection of the line passing through the point “e” in the direction of normal vector \vec{n} and the straight line which connect nodes P and N or E and NE , respectively, $L_{(P',E')}$ stands for the distance between P' and E' . The values of $\phi_{E'}$ and $\phi_{P'}$ can be calculated by using the gradient at the control volume center

$$\phi_{E'} = \phi_E + \nabla\phi_E \cdot (\vec{x}_{E'} - \vec{x}_E), \quad \phi_{P'} = \phi_P + \nabla\phi_P \cdot (\vec{x}_{P'} - \vec{x}_P),$$

where \vec{x}_P , \vec{x}_E , $\vec{x}_{P'}$, and $\vec{x}_{E'}$ are the radius vectors of P , E , P' , and E' , respectively. The k^{th} Cartesian component of $\nabla\phi_P$ are approximated using Gauss's theorem

$$\nabla\phi_P \cdot \vec{i}_k = \left(\frac{\partial\phi}{\partial x_k} \right)_P = \frac{1}{\Delta\Omega} \sum_{c=e,s,n,w} \phi_c S_c^k, \quad S_c^k = S_c (\vec{n} \cdot \vec{i}_k), \quad (3.10)$$

where S_c is the area of “c” control volume face, \vec{n} is the unit outward normal vector to S_c , and \vec{i}_k is the unit basis vector of Cartesian coordinate system $(x_1, x_2) = (x, y)$. Using (3.6) - (3.10) to approximate (3.5), one can determine intermediate velocity fields \vec{u}^* (which is not solenoidal) at each grid nodes even on the boundary.

In the first sub-step the continuity equation (3.3) is not used so that the intermediate velocity field is, in general, non-divergency free. The details of the setting and discretization of the second sub-step developed on non-uniform, collocated grid are now discussed below. Equation (3.2) applies both in continuous and discrete sense. Taking the divergence of both sides of (3.2) and integrating over a control volume Ω , after applying the Gauss theorem and setting the updated velocity filed, \vec{u}^{n+1} , to be divergence free, one gets the equation

$$0 = \frac{1}{\Delta\Omega} \oint_S \vec{u}^{n+1} \cdot \vec{n} dS = \frac{1}{\Delta\Omega} \oint_S \vec{u}^* \cdot \vec{n} dS - \Delta t \frac{1}{\Delta\Omega} \oint_S \nabla p^{n+1} \cdot \vec{n} dS, \quad (3.11)$$

that has to be discretized while collocating the variables in the control volume centers. Here \vec{n} is outward normal to the boundary, S , of control volume Ω . At this stage of the projection procedure, the discrete values of u_x^* and u_y^* are already known and represent the source term in (3.11). A second order discretization of the surface integrals can be obtained by utilizing the mean value formula. This means that a surface integrals in (3.11) can be approximated as

$$\frac{1}{\Delta\Omega} \oint_S \vec{u}^{n+1} \cdot \vec{n} dS \cong \frac{1}{\Delta\Omega} \sum_{c=e,s,w,n} (\vec{u}^{n+1} \cdot \vec{n})_c S_c, \quad (3.12)$$

$$\frac{1}{\Delta\Omega} \oint_S \nabla p^{n+1} \cdot \vec{n} dS \cong \frac{1}{\Delta\Omega} \sum_{c=e,s,w,n} (\nabla p^{n+1} \cdot \vec{n})_c S_c. \quad (3.13)$$

It follows that, by substituting (3.12) and (3.13) into (3.11), one gets the discrete pressure equation

$$\frac{1}{\Delta\Omega} \sum_{c=e,s,w,n} (\vec{u}^* \cdot \vec{n})_c S_c - \frac{\Delta t}{\Delta\Omega} \sum_{c=e,s,w,n} (D_n p^{n+1})_c S_c = 0. \quad (3.14)$$

The iterative method is utilized to approximate $(D_n p^{n+1})_c$ and solve this equation (3.14). The normal-to-face intermediate velocities $(\vec{u}^* \cdot \vec{n})_c$, $c = e, s, w, n$ are not directly available. They are found using interpolation. The derivative of pressure with respect to the direction of the outward normal \vec{n} through the cell face “ c ”, $(D_n p)_c^{n+1}$ is approximated by an iterative technique (see for example Muzaferija, 1994) to reach higher order of approximation and preserved compact stencil in the discrete equation (3.14). Only the east face of a 2D control volume shown in Figure 3.1 will be considered. The same approach applies to other faces. Using second upper index “ s ” to denote the number of iteration one writes

$$\begin{aligned} (D_n p)_e^{n+1,s+1} &= (D_\xi p)_e^{n+1,s+1} + [(D_n p)_e - (D_\xi p)_e]^{n+1,s}, \quad s = 0, \dots, \widehat{S}, \\ (D_n p)^{n+1,0} &= (D_n p)^n, \end{aligned} \quad (3.15)$$

where ξ is the direction along the grid line connecting nodes P and E (see Figure 3.1 a)). The terms in the square brackets are approximated with high-order

and are evaluated by using known values from the previous iteration. Once the iterations converge, the low order approximation term $(D_{\xi p})_e^{n+1,s+1}$ drop out and the obtained solution corresponds to the higher order of approximation. The derivatives of pressure in the square brackets are written as

$$(D_n p)_e^{n+1,s} = (\nabla p \cdot \vec{n})_e^{n+1,s}, \quad (D_{\xi p})_e^{n+1,s} = (\nabla p \cdot \vec{\xi})_e^{n+1,s},$$

where \vec{n} is the unit outward normal vector to cell face “e”, and $\vec{\xi}$ is the unit vector in ξ direction from point P to E . The term $(\nabla p)_e^{n+1,s}$ is approximated similar to (3.9)

$$(\nabla p)_e^{n+1,s} = \left(\sum_l L_{(e,l)}^{-2} \nabla p_l^{n+1,s} \right) / \left(\sum_l L_{(e,l)}^{-2} \right), \quad l = N, P, S, SE, E, NE,$$

where $\nabla p_l^{n+1,s}$ is the gradient of pressure at grid node l and $L_{(e,l)}^{-2} = 1/[(x_e - x_l)^2 + (y_e - y_l)^2]$. The k^{th} component of $\nabla p_l^{n+1,s}$ are discretized by using Gauss theorem (for example at grid node P)

$$\nabla p_P^{n+1,s} \cdot \vec{i}_k = \left(\frac{\partial p^{n+1,s}}{\partial x_k} \right)_P \cong \frac{1}{\Delta\Omega} \sum_{c=e,s,n,w} p_c^{n+1,s} S_c^k, \quad S_c^k = S_c(\vec{n} \cdot \vec{i}_k).$$

The first term in the right hand side of equation (3.15) is treated implicitly, and a simple approximation is used (that gives a compact stencil),

$$(D_{\xi p})_e^{n+1,s+1} \approx \frac{p_E^{n+1,s+1} - p_P^{n+1,s+1}}{L_{(P,E)}},$$

where $L_{(P,E)}$ is the distance between nodes P and E . The final expression for the approximation to the derivative of pressure with respect to \vec{n} through the cell face “e” (3.15) can now be written as

$$(D_n p)_e^{n+1,s+1} = \frac{p_E^{n+1,s+1} - p_P^{n+1,s+1}}{L_{(P,E)}} + \nabla p^{n+1,s} \cdot (\vec{n} - \vec{\xi})_e. \quad (3.16)$$

The terms labelled “ $n + 1, s$ ” become zero when $\vec{\xi} = \vec{n}$, is required. Repeating steps similar to (3.15) - (3.16) for other faces of control volume and substitute result into (3.14), one generates the equation for finding the pressure at next iteration

$(n + 1, s + 1)$

$$\begin{aligned} & \frac{1}{\Delta\Omega} \sum_{c=e,s,w,n} (\vec{u}^* \cdot \vec{n})_c S_c - \frac{\Delta t}{\Delta\Omega} \sum_{c=e,s,w,n} (\nabla p^{n+1,s})_c (\vec{n} - \vec{\xi})_c = \\ & \frac{\Delta t}{\Delta\Omega} \left\{ \left(\frac{p_E - p_P}{L_{(E,P)}} \right)^{n+1,s+1} - \left(\frac{p_P - p_W}{L_{(P,W)}} \right)^{n+1,s+1} + \right. \\ & \left. \left(\frac{p_N^{n+1,s} - p_P^{n+1,s+1}}{L_{(N,P)}} \right) - \left(\frac{p_P - p_S}{L_{(P,S)}} \right)^{n+1,s+1} \right\}. \end{aligned}$$

We use $p_N^{n+1,s}$ instead $p_N^{n+1,s+1}$ to make matrix of algebraic system to be tri-diagonal.

Implementation of Boundary conditions

The Finite volume method requires the boundary fluxes for each control volume either be known or expressed through the known quantities and interior nodal values.

Impermeable wall: The following condition is prescribed on impermeable wall

$$\vec{u} = \vec{u}_{wall}. \quad (3.17)$$

This condition follows from the fact that viscous fluid sticks to a solid wall. Since there is no flow through the wall, mass fluxes, and convective fluxes of all quantities are zero. Diffusive fluxes in the momentum equation are approximated using known boundary values of the unknown and one-sided finite difference approximation for the gradients.

Through-flow part: The implementation of three kinds boundary conditions on the through-flow parts are addressed here. Only the case where east face of control volume aligns with through-flow boundary Γ^1 will be considered. A sketch of the grid and the notations used are shown in Figure 3.1 b). Other faces treated similar.

(a) The velocity is set up (see equation (2.7))

$$\vec{u}_{\Gamma^1} = \vec{u}_p. \quad (3.18)$$

Since the velocity vector is given, the mass flow rate and the convective fluxes can be calculated directly. The diffusive fluxes are not known, but they are approximated

using known boundary values of the unknowns and one-sided finite difference approximation for the gradient. It is important to note how boundary condition (3.18) is involved in the derivation of the discrete pressure equation. Because $(\bar{u}^{n+1})_e$ is given by (3.18) the approximation of equation (3.11) becomes

$$\frac{1}{\Delta\Omega} \left[(\bar{u}^{n+1} \cdot \bar{n})_e + \sum_{c=s,w,n} (\bar{u}^* \cdot \bar{n})_c S_c \right] - \frac{\Delta t}{\Delta\Omega} \sum_{c=s,w,n} (D_n p^{n+1})_c S_c = 0.$$

One does not need to approximate $(D_n p^{n+1})_e$ at face “e”. However, if pressure at the boundary Γ^1 is needed at some stage, it can be obtained by extrapolation within the domain.

(b) The tangential velocity and pressure are prescribed (see equation (2.6))

$$(\vec{u} \cdot \vec{\tau})_{\Gamma^1} = G(x, y, t), \quad p_{\Gamma^1} = H(x, y, t), \quad (x, y) \in \Gamma^1. \quad (3.19)$$

When the tangential velocity and pressure are specified on the through-flow part of boundary, the mass and convective fluxes are not known. One has to find them during the solution process. The solenoidal constraint, $\nabla \cdot \vec{u} = 0$ has to be applied at the boundary where the pressure is specified. Because the through-flow boundary may not be aligned with the Cartesian coordinates, we shall refer to the local coordinates system (n, τ) , which is a rotated Cartesian frame with n in the direction of normal vector to the through-flow boundary and τ in the direction of the tangential vector to the through-flow boundary. The velocity vector $\vec{u} = (u_x, u_y)$ can be expressed in terms of velocity components in local orthogonal coordinates $\vec{u} = (U_n, U_\tau)$, where $U_n = \vec{u} \cdot \bar{n}$ is the normal velocity component to the through-flow boundary, $U_\tau = \vec{u} \cdot \bar{\tau}$ is the tangential velocity component to the through-flow boundary which is known at Γ_1 from boundary condition (3.19). The continuity equation in terms of local orthogonal coordinates (n, τ) reads

$$\frac{\partial U_n}{\partial n} + \frac{\partial U_\tau}{\partial \tau} = 0. \quad (3.20)$$

Using equation (3.19) and (3.20) yields

$$\left(\frac{\partial U_n}{\partial n}\right)_{\Gamma^1} = -\frac{\partial G}{\partial \tau}. \quad (3.21)$$

To find the flux on the through-flow part, one needs to calculate the normal velocity $(U_n)_e$ at the east cell face “e” (See Figure 3.1 (b)). The normal derivative of U_n at the east cell face is approximated by one-side difference

$$\left(\frac{\partial U_n}{\partial n}\right)_{e'} = \frac{(U_n)_{e'} - (U_n)_P}{L_{(e',P)}}, \quad (3.22)$$

where e' is a point of intersection of line passing through node P parallel to normal vector to Γ^1 and the line coincide with boundary Γ^1 (see Figure 3.1 b)). Following equation (3.21) and (3.22), the normal velocity component at point e' is approximated as

$$(\vec{u}^{n+1} \cdot \vec{n})_{e'} = (U_n^{n+1})_{e'} = (U_n^{n+1})_P - L_{(e',P)} \left(\frac{\partial G}{\partial \tau}\right)_{e'}. \quad (3.23)$$

The discreet pressure equation for control volume Ω near through-flow boundary has the following form

$$\frac{1}{\Delta \Omega} \left[(\vec{u}^{n+1} \cdot \vec{n})_{e'} S_e + \sum_{c=s,w,n} (\vec{u}^* \cdot \vec{n})_c S_c \right] - \frac{\Delta t}{\Delta \Omega} \sum_{c=s,w,n} (D_n p^{n+1})_c S_c = 0. \quad (3.24)$$

Here, point “e'” is used instead “e” to approximate flux through east face. In this case the order of approximation is reduced to first order. Moreover, in many case, the grid is arrange such that “e'” coincide with center of east face. Substituting (3.23) into (3.24) and utilizing (3.11) at node P yields

$$\begin{aligned} & \frac{1}{\Delta \Omega} \left[(\vec{u}^* \cdot \vec{n})_P - \Delta t (\nabla p^{n+1,s+1} \cdot \vec{n})_P - L_{(e',P)} \frac{\partial G}{\partial \tau} \right] S_e + \\ & \frac{1}{\Delta \Omega} \left[\sum_{c=s,w,n} (\vec{u}^* \cdot \vec{n})_c S_c \right] - \frac{\Delta t}{\Delta \Omega} \sum_{c=s,w,n} (D_n p^{n+1,s+1})_c S_c = 0. \end{aligned}$$

The derivative of pressure with respect to outward normal direction n at node P approximated by one-side difference

$$(D_n p)_P^{n+1,s+1} = \frac{p_{e'}^{n+1} - p_P^{n+1,s+1}}{L_{(P,e')}},$$

where $L_{(P,e')}$ is the distance between nodes P and e' on the boundary Γ^1 .

(c) The tangential velocity and total pressure are prescribed (see equation (2.5)) by

$$(\vec{u} \cdot \vec{\tau})_{\Gamma^1} = G, \quad p + \frac{1}{2}|\vec{u}|^2 = H(x, y, t), \quad (x, y) \in \Gamma^1. \quad (3.25)$$

When the tangential velocity and total pressure are specified on the through-flow part, the situation arises where mass flux, convective flux, and pressure are not known. Let us use local coordinates system (η, τ) as in the previous case. The flux $(U_n)_{e'} = (\vec{u} \cdot \vec{n})_{e'}$ is approximated by equation (3.23). Since the pressure term on the through-flow boundary Γ^1 (see Figure 3.1 b)) is unknown, one needed to approximate the pressure on the through-flow part by using the total pressure boundary condition, and one needs to calculate the pressure at point e' . The total pressure on through-flow part can be expressed in terms of local orthogonal coordinates (n, τ) in $2D$ at point e' as

$$p_{e'}^{n+1,s+1} + \frac{1}{2}|U_{e'}^{n+1}|^2 = p_{e'}^{n+1,s+1} + \frac{1}{2}((U_n^{n+1})_{e'}^2 + (U_\tau)_{e'}^2) = H.$$

Using boundary condition (3.25) the last equation recasts as

$$p_{e'}^{n+1,s+1} + \frac{1}{2}(U_n^{n+1})_{e'}^2 = H - \frac{1}{2}G_{e'}^2.$$

Substituting $(U_n^{n+1})_{e'}$ given by (3.23) yields

$$p_{e'}^{n+1,s+1} + \frac{1}{2} \left((U_n^{n+1})_P - \frac{L_{(e',P)}}{2} \frac{\partial G}{\partial \tau} \right)^2 = H - \frac{1}{2}G_{e'}^2.$$

Using $(U_n^{n+1})_P = (\vec{u}^{n+1} \cdot \vec{n})_P = (\vec{u}^* \cdot \vec{n})_P - \Delta t(\nabla p^{n+1,s+1} \cdot \vec{n})$ yields

$$p_{e'}^{n+1,s+1} + \frac{1}{2} \left[(\vec{u}^* \cdot \vec{n})_P - \Delta t(\nabla p^{n+1,s+1} \cdot \vec{n})_P - L_{(e',P)} \frac{\partial G}{\partial \tau} \right]^2 = H - \frac{1}{2}G_{e'}^2. \quad (3.26)$$

Dropping terms of order $O(\Delta t)$ one gets

$$p_{e'}^{n+1,s+1} = H - \frac{1}{2}G_{e'}^2 - \frac{1}{2}(\vec{u}^* \cdot \vec{n})_P^2 - \frac{1}{2}L_{(e',P)}^2 \left(\frac{\partial G}{\partial \tau} \right)_{e'}^2 + (\vec{u}^* \cdot \vec{n})_P L_{(e',P)} \left(\frac{\partial G}{\partial \tau} \right)_{e'}.$$

We have the previous case where pressure is given on the through-flow parts. When on the through-flow boundary $\vec{n} = \vec{\xi}$ and $G = 0$, the expression for p_e (3.26) reads

$$p_e^{n+1,s+1} = H - (\vec{u}^* \cdot \vec{n})_P^2.$$

Overall Solution Method

The steps in the numerical solution algorithm can be summarized as follows.

- Starts with velocity at time step n which is satisfied with an incompressibility constrain.
- Construct and solve the equation for the intermediate velocity (3.5) by using equations (3.6) - (3.10). This velocity field do not satisfy an incompressibility constraint. The finite volume method requires that the boundary fluxes either be known or expressed in term of known quantities. Since the initial data for velocity at step time n is given then all fluxes can be calculated. If the velocity on the boundary is not known, it is easy to find approximation of velocity on the boundary. Usually one extrapolates along grid line from the interior boundary. All the convective fluxes and diffusive fluxes can be calculated.
- In the second sub-step, it is needed to find pressure at time step $n + 1$. To construct and solve the equation to find pressure, we start with an integral form of an incompressibility constrain on each control volume. Using equations (3.11)-(3.16), one generates the equation to find pressure. The construction of this equations followed by the idea of Muzaferija (1994) which carried out by using the iteration process. On this step, there are three kinds of boundary condition on the through-flow parts (2.5)-(2.7). The implementation of pressure equation for three kinds of boundary conditions on through-flow part are investigated and shown in the part of **Implementation of boundary conditions**. The pressure at step time $n + 1$ achieved as condition is fulfilled

$$\|p^{n+1,s+1} - p^{n+1,s}\| \leq \varepsilon = 10^{-4}.$$

- Construct and solve the discretization for the velocity at time step $n + 1$. Since all quantities (intermediate velocity and pressure at time step $n + 1$) are known, the velocity at time step $n + 1$ is achieved.

3.2 Validation Test

In this section the numerical method is validated by comparison analytical and numerical solutions for the laminar flow driven by pressure drop in the $2D$ plane channel and the $2D$ gap between two cylinders. The details of each problem and computed results are discussed.

3.2.1 Flow between two parallel plates

The purpose of this test is to estimate the potential and quality of developed method in the case of unsteady flow. Consider the two-dimensional channel flow between two parallel plates. The Cartesian coordinate system (x, y, z) is chosen so that the x -axis is taken as the direction of flow, y is the coordinate normal to the plate, z is the coordinate normal to x and y , respectively. The velocity field is assumed in the form $\vec{u} = u(y, t)\vec{i}$, where u is the velocity in the x -coordinate direction, \vec{i} is the unit vector in the x -coordinate direction. The Navier-Stokes equations implies that the pressure gradient is a function of time only $\partial p / \partial x = f(t)$.

Initial data at $t = 0$ is the fluid at rest, $u(y, 0) = 0$. The flow is driven by pressure different $p_2(0, t) - p_1(L, t) = \Delta p \cos(\omega t)$ where L is length between through-flow parts, ω is frequency, and Δp is the characteristic pressure difference between through-flow parts AB and CD . The problem is dimensionalized with height of channel, h , as the length scale, $\Delta p h / L$ as the pressure scale, $\sqrt{\Delta p h} / \sqrt{\rho L}$ as the velocity scale, and $\sqrt{\rho h L} / \sqrt{\Delta p}$ as the time scale. Non-dimensional frequency is $\eta = \omega \sqrt{\Delta p} / \sqrt{\rho h L}$. Since the flow is driven by pressure difference and there is no

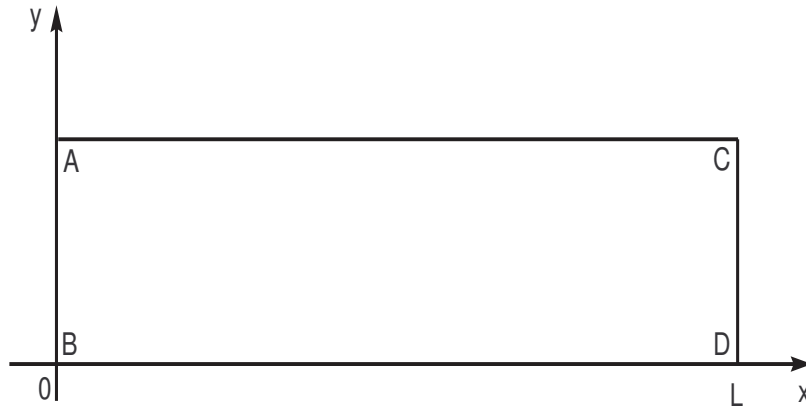


Figure 3.2 Sketch of the problem. Flow between two parallel plates.

velocity scale in the problem, we use $\rho U^2 = \Delta p h / L$ in the traditional definition of the Reynolds number, and call it as “*Pressure Reynolds Number*”

$$Re_{\Delta p} = \frac{U h}{\nu} = \frac{h}{\nu} \sqrt{\frac{\Delta p h}{\rho L}}$$

where ν is the kinematic viscosity. The analytical solution of dimensionless problem obtained by separation of variables is (see Appendix A)

$$u(y, t) = \sum_{n=1}^{\infty} \left\{ b_n \sin(n\pi y) \int_0^t e^{-\lambda_n^2(t-\tau)} \cos(\eta\tau) d\tau \right\}, \quad (3.27)$$

$$\lambda_n = \frac{n\pi}{\sqrt{Re}}, \quad b_n = \frac{2[1 - \cos(n\pi)]}{n\pi}, \quad n = 1, 2, \dots$$

Computations are carried out with 1,000 cells distributed in a uniform manner in the channel. A uniform grid having 20 lines across the channel and 50 lines in the direction of x was found to reproduce with satisfactory accuracy the flow parameters. In order to reduce computer cost, the distance between through-flow parts was chosen to be one, $L = 1$. The dependence between Re_Q and $Re_{\Delta p}$ is plotted in Figure 3.3, for constant pressure drop $P_2(L, t) - P_1(0, t)$. The solid lines represent exact relation $Re_Q = Re_{\Delta p}^2 / 12$ where $Re_Q = Q / \nu$ is the Reynolds number based on the flow rate, $Q = \int_0^1 u(y) dy$. Circle signs represent the results of our numerical simulations. The Reynolds number Re_Q is not known a priori, it was computed at the end of the numerical simulation from the steady state flow rate obtained with the given $Re_{\Delta p}$.

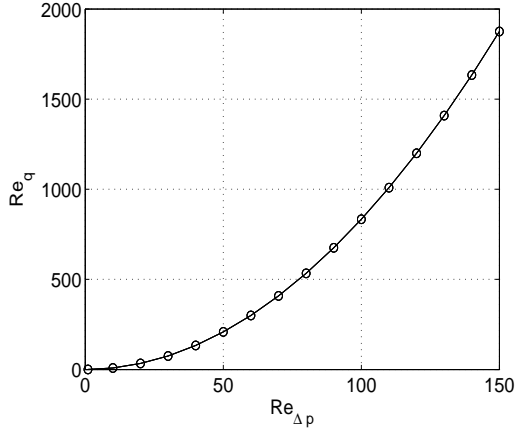


Figure 3.3 The relation between Re_Q and $Re_{\Delta p}$.

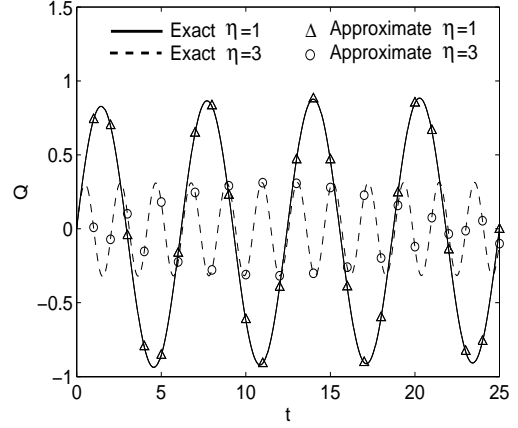


Figure 3.4 Volume rate vs time, $Re_{\Delta p} = 150$.

As expected, the results are very close and the velocity profile for all cases was the parabolic Poiseuille flow. From the analytical solution given by (3.27), it is obvious that the mass flow rate oscillation is function of oscillating frequency η and the pressure Reynolds number, $Re_{\Delta p}$. In Figure 3.4 the variation of $Q(t) = \int_0^1 u(y, t) dy$ with time t is shown for $\eta = 1$ and 3, and $Re_{\Delta p} = 150$. Solid line and dash line represent exact solution for $\eta = 1, 3$, respectively. Circle signs and triangle signs correspond to the result of our numerical simulations for $\eta = 1$ and 3, respectively. The numerical solution starts at $t = 0$ and the time step is $\Delta t = 10^{-4}$. The above result corroborated that proposed numerical method successfully predicts the volume rate for the constant and oscillated pressure drop.

3.2.2 Flow with Circular Streamline

Another simple type of fluid motion through a bounded domain is one in which all the streamlines are circles centered on a common axis of symmetry. Steady motion can be generated by a circumferential pressure gradient in the domain between two concentric cylinders of radii r_1 and r_2 . If the motion is to remain purely rotatory

with the axial component of velocity to be zero, the axial pressure gradient must be zero, and the Navier-Stokes equation show that motion must be two-dimensional. Using the equation of motion in polar coordinates (r, θ) and assuming that velocity component in the direction of the θ -coordinate line $v = v(r)$ is a function of r only, and the radial velocity component is zero, one finds

$$\frac{v^2}{r} = \frac{\partial p}{\partial r}, \quad (3.28)$$

$$\frac{\partial^2 v}{\partial r^2} + \frac{1}{r} \frac{\partial v}{\partial r} - \frac{v}{r^2} = \frac{1}{r} \frac{\partial p}{\partial \theta}. \quad (3.29)$$

Equation (3.28) and (3.29) dimensionless with $h = r_2 - r_1$ as length scale, ν/h as velocity scale, $\rho\nu^2/h^2$ as pressure scale, and $d_0 = (r_1 + r_2)/(2h) = R_0/h$ is non-dimensional radius of centerline. Figure 3.5 represents sketch of the problem geometry

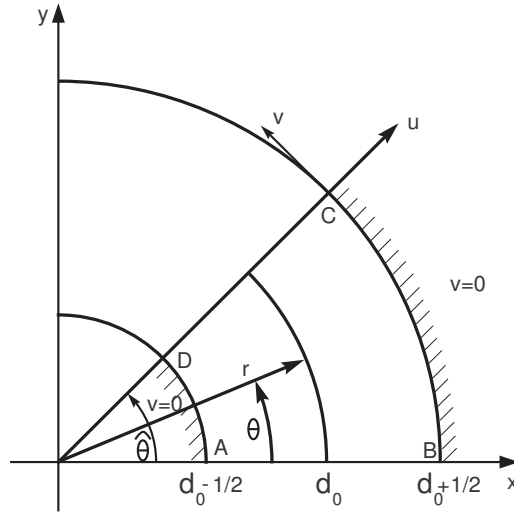


Figure 3.5 Sketch of problem domain. Circular streamline.

and main notations. It is easy to see from (3.28) and (3.29) that pressure has to be a linear function of θ ,

$$p(r, \theta) = f(r) + K\theta, K = \frac{\partial p}{\partial \theta} = \text{const}, f(r) = \int_{d_0 - \frac{1}{2}}^r \frac{v^2(\xi)}{\xi} d\xi.$$

With the boundary condition

$$v \leq (d_0 \pm \frac{1}{2}) = 0, \quad (3.30)$$

one obtains solution of (3.28)-(3.30) in the following form

$$v(r) = \frac{K}{8} \left\{ C_1 r + \frac{C_2}{r} + 4r \ln r \right\}, \quad d_0 - \frac{1}{2} \leq r \leq d_0 + \frac{1}{2}, \quad (3.31)$$

$$p(r, \theta) = \int_{d_0 - \frac{1}{2}}^r \frac{v^2(\xi)}{\xi} d\xi + K\theta, \quad 0 \leq \theta \leq \hat{\theta}, \quad d_0 - \frac{1}{2} \leq r \leq d_0 + \frac{1}{2}, \quad (3.32)$$

$$C_1 = \frac{(2d_0 - 1)^2 \ln(d_0 - \frac{1}{2}) - (2d_0 + 1)^2 \ln(d_0 + \frac{1}{2})}{2d_0}, \quad (3.33)$$

$$C_2 = \frac{(4d_0^2 - 1)^2}{8d_0} \ln \left(\frac{d_0 + \frac{1}{2}}{d_0 - \frac{1}{2}} \right). \quad (3.34)$$

The non-dimensional volume rate of flow becomes

$$Q = \int_{d_0 - \frac{1}{2}}^{d_0 + \frac{1}{2}} v dr = \frac{K}{8} E, \quad (3.35)$$

$$E = 2C_1 d_0 + C_2 \ln \left(\frac{d_0 + \frac{1}{2}}{d_0 - \frac{1}{2}} \right) - 4d_0 + 2\left\{ (d_0 + \frac{1}{2})^2 \ln(d_0 + \frac{1}{2}) - (d_0 - \frac{1}{2})^2 \ln(d_0 - \frac{1}{2}) \right\}. \quad (3.36)$$

Problem (3.28) - (3.30) can be considered as example of flowing through problem where pressure and tangent component of the velocity vector are given on through-flow parts AB and DC . It worth to note here that distribution of pressure is not constant at the through-flow parts and that numerical solution uses the Navier-Stokes equation in the terms of Cartesian coordinates and Cartesian velocity components $\vec{u} = (u_x, u_y)$ where $u_x = -v(r) \sin(\theta)$, $u_y = v(r) \cos(\theta)$, $r^2 = x^2 + y^2$, and $\theta = \arctan(y/x)$. Using exact solution (3.31)-(3.34), one can formulate flowing through problems where total pressure, $p + \frac{1}{2} [u_x^2(r, \theta) + u_y^2(r, \theta)]$, and tangent velocity are known on through-flow parts or velocity vector is known $v(r, 0) = v(r)$, $u = 0$. It is also possible to consider problem where in through-flow parts, different kinds of boundary conditions are holds. The test cases of flowing through problems computed in this section are summarized in Table 3.1. In all cases we use $0 \leq \theta \leq \pi$. Non-orthogonal logically rectangular boundary-fitted grid were constructed as follows. The impermeable boundaries AD and CB equally partitioned on M subintervals.

Case	through-flow		solid wall
	$AB(\theta = 0)$	$CD(\theta = \pi)$	$AD, CB(0 \leq \theta \leq \pi)$
1	$u_x = 0, p = f(r)$	$u_x = 0, p = f(r) + K\pi$	$u_x = u_y = 0$
2	$u_x = 0, u_y = v(r)$	$u_x = 0, p = f(r) + K\pi$	$u_x = u_y = 0$
3	$u_x = 0, u_y = v(r)$	$u_x = 0, p + \frac{1}{2}u_y^2 = H(r)$	$u_x = u_y = 0$
4	$u_x = 0, p = f(r)$	$u_x = 0, p + \frac{1}{2}u_y^2 = H(r)$	$u_x = u_y = 0$

Table 3.1 Test cases $0 \leq \theta \leq \pi$, $\vec{u} = (u_x, u_y)$, and $H(r) = p + \frac{1}{2}u_y^2$.

Grid	$\ v^{app} - v^{ext} \ $			
	case 1	case 2	case 3	case 4
20×10	1.508E-01 -	1.220E-01 -	1.218E-01 -	1.425E-01 -
40×20	3.979E-02(1.92)	3.026E-02(2.01)	3.018E-02(2.01)	3.753E-02(1.93)
80×40	9.955E-03(1.99)	8.291E-03(1.87)	7.590E-03(1.99)	9.739E-03(1.95)

Table 3.2 Rate of convergence. Four test cases, $K = 500$.

The flowing thought parts AB and CD divided into an equal number of N subintervals. The grid independence study has been carried out for several values of circumferential pressure gradient, K , and for four cases of the flowing through problems. The influence of the grid size on the difference between the exact velocity (3.31) and the approximate velocity in the maximum norm is shown in Table 3.2 for $K = 500$. The convergence rates for the two finest grid are compared to the next coarser grid (see value in the brackets). Upper indices “*ext*” and “*app*” reference the exact and approximate solutions, respectively. It can be clearly seen from these result that the rate of convergence is near two. For Case 1, Figure 3.7 shows the variation of the dimensionless x -component of the velocity vector along the line $\theta = \pi/2$ with the circumferential pressure gradient $\partial p / \partial \theta = K$. The value of circumferential pressure

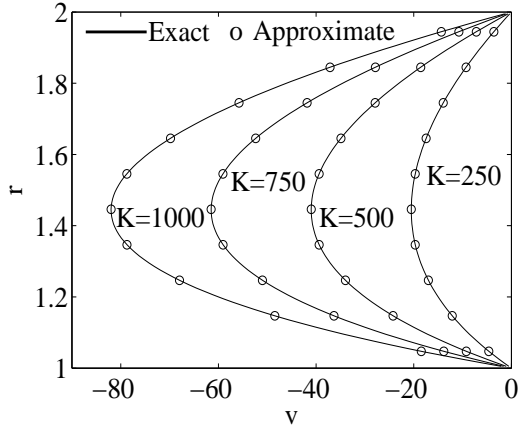


Figure 3.6 Velocity profile at the vertical line $\theta = \pi/2$ (component u_x) for the Case 1 and different values of K .

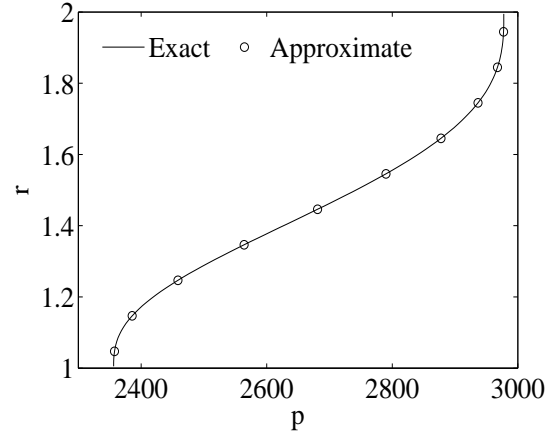


Figure 3.7 Pressure along the line $\theta = \pi/2$, $K = 500$ for Case 1.

gradient varies from $K = 250$ to $K = 1000$. Figure 3.6 shows pressure distribution for the Case 1 along the line $\theta = \pi/2$ and $K = 500$. In both figures the solid lines represent the exact solution (3.31) and (3.32) and the circle signs represent the numerical results. The calculated velocity profile and pressure along the line $\theta = const$ for the Cases 2-4 are also in excellent agreement with exact solution.

CHAPTER IV

FLOW IN PLANAR T-JUNCTION CHANNEL

The flow through branching channels has been widely used in engineering construction, such as piping systems and ventilation systems, and is encountered in human bodies, for examples blood flows in veins and arteries. The mechanics of such flow are complex and not well understood exhibiting nontrivial flow patterns which include zone of recirculation and stream wise vortex. The vascular system depends on the branches to distribute blood. The arterial wall in the branching regions are exposed to high and low shear stress which disturb local mass transfer and cause cell degradation. Therefore, the atherosclerosis occurs mainly in these regions. In this context, an important and a most popular flow geometry is the flow in bifurcating 90° T-junction.

In large number of numerical and experimental investigations on viscous incompressible flow in bifurcating T-junction both Newtonian and non-Newtonian fluids are considered. The flow is analyzed in terms of topology pattern, particle path and wall shear stress. Let us mention just several of more recent papers providing sufficiently complete review and dealing with this problem.

A computational method for the prediction of incompressible flow in domain with specified pressure boundaries is developed in Kelkar and Choudhury (2000). The proposed method is applied for predicting incompressible forced flow in branched ducts. Fully developed velocity boundary conditions (i.e. a parabolic profile) are applied at the inlet, and constant pressure boundary condition are applied at the exit of the two downstream channels of planar T-shape and Y-shape branch configurations.

A numerical predictions of the laminar fluid flow and heat transfer charac-

teristics in planar (two-dimensional) impacting tee junctions have been reported by El-Shbourny *et al.* (2003). The numerical solution of the governing equations was obtained using CFX-TASC flow package. Fully developed velocity and temperature profiles were assumed at the inlet face of the impacting junction. The results include wall shear stress distributions, streamlines showing the number, location, and size of the re-circulation zones, the pressure loss coefficient, wall heat flux distributions, isotherms, and the overall rate of heat transfer.

The unsteady flow in a square tube T-junction with a time-dependent periodic inlet flow rate (zero to a maximum value) and equal branch flow rates is examined in Anagnostopoulos (2004). The simulation algorithm is based on the finite volume approach and uses Cartesian, collocated grid structures. No slip conditions are set at all tube walls, whereas Neumann conditions are applied at the inlet and outlet sections for the flow velocity, combined with mass balancing to correct the normal velocity component, according to the flow rate wave form. The same flow rate wave form, divided by 2, is applied at the exit of each tube branch, since it was assumed from the beginning that the flow always divides equally among the two branches. Hence, all the boundary values for the fluid velocity are specified for each time instant.

In the study of Tsui (2006) a numerical method is employed to examine the flow in symmetrical, two-dimensional branches of Y shape and Tee shape. The methodology is based on a pressure-correction procedure within the frame of unstructured grids. Specified pressures are imposed at the outlet of the two branches. The area ratio of the branch is allowed to vary in the range of 2-3. The effects of slightly different pressures prescribed on the outlets are investigated.

An investigation of laminar steady and unsteady flows in a two-dimensional T-junction was carried out by Miranda *et al.* (2008) for Newtonian and a non-Newtonian fluid analogue to blood. Under steady flow, calculations were performed for a wide range of Reynolds numbers and extraction flow rate ratios, and accurate

data for the recirculation sizes were obtained and are tabulated. At the inlet, the stream wise velocity component and the shear stress component are prescribed, based on available analytical solutions. The velocity follows a parabolic shape for the steady flows and the Womersley solution for the pulsating flows. At the walls the no-slip condition is applied directly, as a Dirichlet condition, and the shear stress is calculated from the local velocity distribution. At the two outlets of the T-junction the flow rates in each of the outlets are prescribed.

What is clear from these short reviews is the lack of work on study flows of fluids through T-junction in case where pressure difference between branches are only known and the flow within domain needs to be determined.

There are three types of boundary condition relevant to the present flow problems: inlet, outlets, and solid walls. As a rule at the inlet, the stream wise velocity component is prescribed, based on available analytical solutions. At the solid walls, the no-slip condition is applied. At the outlets (may be more than two) of the junction, either the pressure is prescribed, and the flow split, or the flow rates in each of the outlets are prescribed. In all these cases the direction of the flow at the domain boundary is assumed to be known.

Antontsev *et al.* (1990), Ragulin (1976), and Ragulin *et al.* (1980) have studied initial boundary value problems where on through-flow parts of domain's boundary (inlet and outlet parts) the values of pressure or total pressure are prescribed. In Ragulin (1976) and Ragulin *et al.* (1980) the problem for homogeneous Navier-Stokes equation have been considered. Wellposedness of nonhomogeneous Navier-Stokes equation have been investigated in Antontsev *et al.* (1990). The objective of this work is two fold:

(i) To validate the numerical method proposed in Chapter III by comparing our numerical results with known experimental and computational data for the two dimensional laminar flow through a 90° T-junction channel.

(ii) To analyze the numerical solution in order to elucidate the flow topology patterns depends on pressure drops between branches of planar T-junction channel.

4.1 Validation tests

The T-junction flow geometry is schematically represented in Figure 4.1. The origin of the coordinate system is located in the lower horizontal boundary opposite the left corner of branch as demonstrated. The left hand side branch, the upper branch, the right hand side branch, and the junction area are denoted by Γ_1 , Γ_2 , Γ_3 , and Γ_4 , respectively. All branches have the same width, w . Two flow rate ratio are

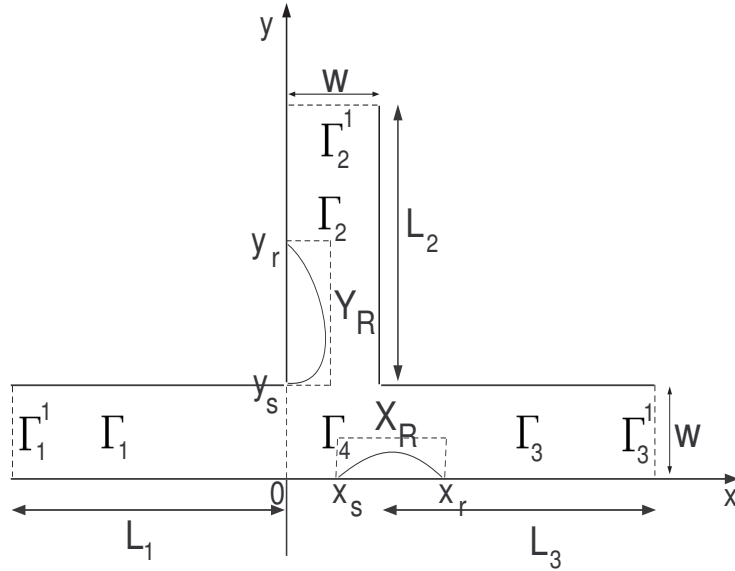


Figure 4.1 Schematic geometry of T-junction bifurcation and coordinate system.

defined as $\beta \equiv Q_2/Q_1$ and $\beta^* \equiv Q_3/Q_1$, where Q_1 , Q_2 , and Q_3 are the inlet duct, branch duct, and right duct flow rates per unit span, respectively. In each duct the bulk velocity is defined as the ratio between the corresponding flow rate and duct width, as in $\bar{u}_1 = Q_1/w$. The main recirculation region is in the branch duct starting at $y = y_s$ and ending at $y = y_r$, thus defining a normalized recirculation length of $Y_R = (y_r - y_s)/w$. This nomenclature is adapted for the secondary recirculation found

in the main duct and aligned with the x -direction with the necessary adaptations leading to $X_R = (x_r - x_s)/w$.

Four kinds of the flowing through problems have been considered in this study. They are the following

- **T1.** On through-flow part Γ_1^1 a laminar, fully developed, parabolic velocity profile is prescribed

$$\vec{u} = (u_x(y), 0), \quad (x, y) \in \Gamma_1^1. \quad (4.1)$$

On through-flow parts Γ_2^1 and Γ_3^1 tangent component of velocity vector and the pressure are specified

$$\vec{u} \cdot \vec{\tau}_2 = u_y = 0, \quad p = p_2, \quad (x, y) \in \Gamma_2^1, \quad (4.2)$$

$$\vec{u} \cdot \vec{\tau}_3 = u_x = 0, \quad p = p_3, \quad (x, y) \in \Gamma_3^1, \quad (4.3)$$

where $\vec{\tau}_i$ is the unit tangent vector to Γ_i^1 , $i = 2, 3$.

- **T2.** On through-flow part Γ_1^1 a laminar, fully developed, parabolic velocity profile is prescribed

$$\vec{u} = (u_x(y), 0), \quad (x, y) \in \Gamma_1^1. \quad (4.4)$$

On through-flow parts Γ_2^1 and Γ_3^1 tangent component of velocity vector and the total pressure are specified

$$\vec{u} \cdot \vec{\tau}_2 = u_y = 0, \quad p + \frac{1}{2}\rho|\vec{u}^2| = H_2(x, y), \quad (x, y) \in \Gamma_2^1, \quad (4.5)$$

$$\vec{u} \cdot \vec{\tau}_3 = u_x = 0, \quad p + \frac{1}{2}\rho|\vec{u}^2| = H_3(x, y), \quad (x, y) \in \Gamma_3^1, \quad (4.6)$$

where $\vec{\tau}_i$ is the unit tangent vector to Γ_i^1 , $i = 2, 3$.

- **T3.** On through-flow part Γ_1^1 a laminar, fully developed, parabolic velocity profile is prescribed

$$\vec{u} = (u_x(y), 0), \quad (x, y) \in \Gamma_1^1. \quad (4.7)$$

On through-flow part Γ_2^1 tangent component of velocity vector and the total pressure are specified

$$\vec{u} \cdot \vec{\tau} = u_y = 0, \quad p + \frac{1}{2}\rho|\vec{u}^2| = H(x, y), \quad (x, y) \in \Gamma_2^1, \quad (4.8)$$

On through-flow part Γ_3^1 tangent component of velocity vector and the pressure are specified

$$\vec{u} \cdot \vec{\tau} = u_x = 0, \quad p = p_3, \quad (x, y) \in \Gamma_3^1, \quad (4.9)$$

where $\vec{\tau}$ is the unit tangent vector to Γ_i^1 , $i = 2, 3$.

- **T4.** On through-flow parts Γ_i^1 , $i = 1, 2, 3$ tangent component of velocity vector and the pressure are specified

$$\vec{u} \cdot \vec{\tau}_i = u_x = 0, \quad p = p_i, \quad (x, y) \in \Gamma_1^i, \quad i = 1, 3, \quad (4.10)$$

$$\vec{u} \cdot \vec{\tau}_2 = u_y = 0, \quad p = p_2, \quad (x, y) \in \Gamma_1^2, \quad (4.11)$$

where $\vec{\tau}_i$ is the unit tangent vector to Γ_i^1 , $i = 1, 2, 3$.

The first set of calculations is compared with those of Hayes *et al.* (1989), Kelkar and Choudhury (2000), and Fluent Inc. (1998). A flowing through problem T1 with $u_x = 4y - 4y^2$, and equal static pressure $p_2 = p_3 = 0$ is considered. The Navier-Stokes equation dimensionlized with the width, w , as characteristic length, the inlet centerline velocity U_c as the characteristic velocity and ρU_c^2 as the scale of pressure. A range of Reynolds number $Re = wU_c/\nu$, where ν is kinematic viscosity is studied with $Re \in [10, 400]$. The computational domain was set to have lengths of $L_1/w = 2$ and $L_2/w = L_3/w = 3$ according to the results represented in Fluent Inc. (1998). The square meshes containing 20, 30, and 40 cells from wall to wall are used. The studied cases start from motionless state. A steady flow achieved as condition is fulfilled

$$\|\vec{u}^{n+1} - \vec{u}^n\| \leq \varepsilon = 10^{-8}.$$

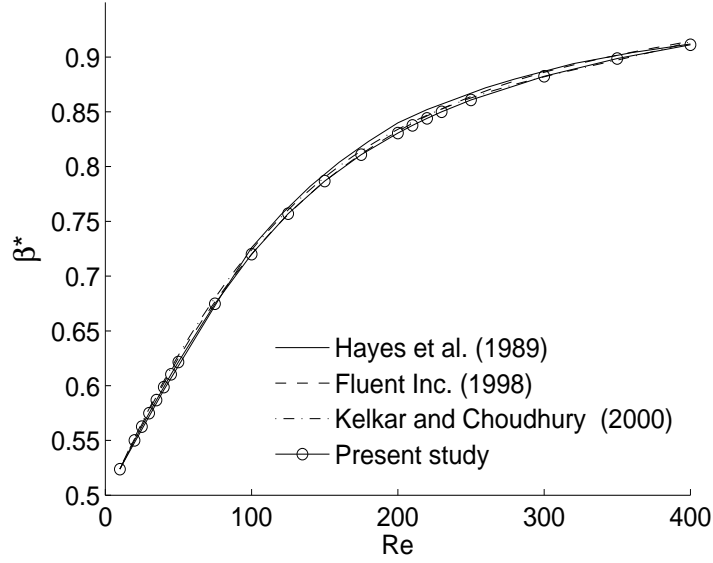


Figure 4.2 The flow rate ratio, β^* , as a function of Reynolds number, Re .

The maximum norm in the set of grid functions is used. Figure 4.2 shows the effect of increasing Reynolds number on the flow rate ratio between the main and the side exit branches. The value of β^* increase from 0.5 for small Reynolds number, $Re < 10$, to about 0.9 at $Re = 400$. In Table 4.1, the flow split predicted by the present method in the sequence of grids are compared with the computation results of Fluent Inc. (1998) software. Three square grids are considered. The details of meshes are given in Table 4.1. Figure 4.3 shows the predicted streamline pattern and pressure contour plots for four Reynold Numbers $Re = 100, 200, 300, 400$. Flow separation from the left wall of the upper branch occurs at all considered Reynolds numbers. These are very similar to those reported in Fluent Inc. (1998). The size and extent of flow separation zone are in a good agreement with results of Hayes *et al.* (1989), Kelkar and Choudhury (2000), and Fluent Inc. (1998).

The second set of calculations is compared with experiments of Liepsch *et al.* (1982) and numerical calculations of Miranda *et al.* (2008). Experimental case of Liepsch *et al.* (1982) pertains to a Reynolds number of 248 ($Re_Q \equiv \rho \bar{u}_1 w / \mu$, $\bar{u}_1 = Q_1/w$ is the bulk velocity) and fixed flow rate ratio $\beta = 0.44$. The relation between

Reynolds numbers, Re		10	100	200	300	400
	Fluent	0.668	0.668	0.668	0.668	0.668
Total mass	$h_1 = 1/20$	0.670	0.670	0.670	0.670	0.670
flow rate	$h_2 = 1/30$	0.668	0.668	0.668	0.668	0.668
	$h_3 = 1/40$	0.667	0.667	0.667	0.667	0.667
	Fluent	0.319	0.187	0.112	0.077	0.057
Upper branch	$h_1 = 1/20$	0.320	0.186	0.112	0.078	0.059
mass flow rate	$h_2 = 1/30$	0.319	0.186	0.112	0.077	0.058
	$h_3 = 1/40$	0.320	0.186	0.112	0.078	0.059
	Fluent	0.350	0.481	0.556	0.592	0.611
Right branch	$h_1 = 1/20$	0.350	0.484	0.558	0.592	0.611
mass flow rate	$h_2 = 1/30$	0.348	0.482	0.556	0.591	0.610
	$h_3 = 1/40$	0.347	0.481	0.555	0.589	0.608
	Fluent	0.524	0.720	0.832	0.886	0.914
Flow slit in	$h_1 = 1/20$	0.522	0.722	0.833	0.884	0.912
Right side branch	$h_2 = 1/30$	0.521	0.721	0.832	0.884	0.913
	$h_3 = 1/40$	0.520	0.721	0.832	0.883	0.912

Table 4.1 Flow split, $Re = 10, 100, 200, 300, 400$.

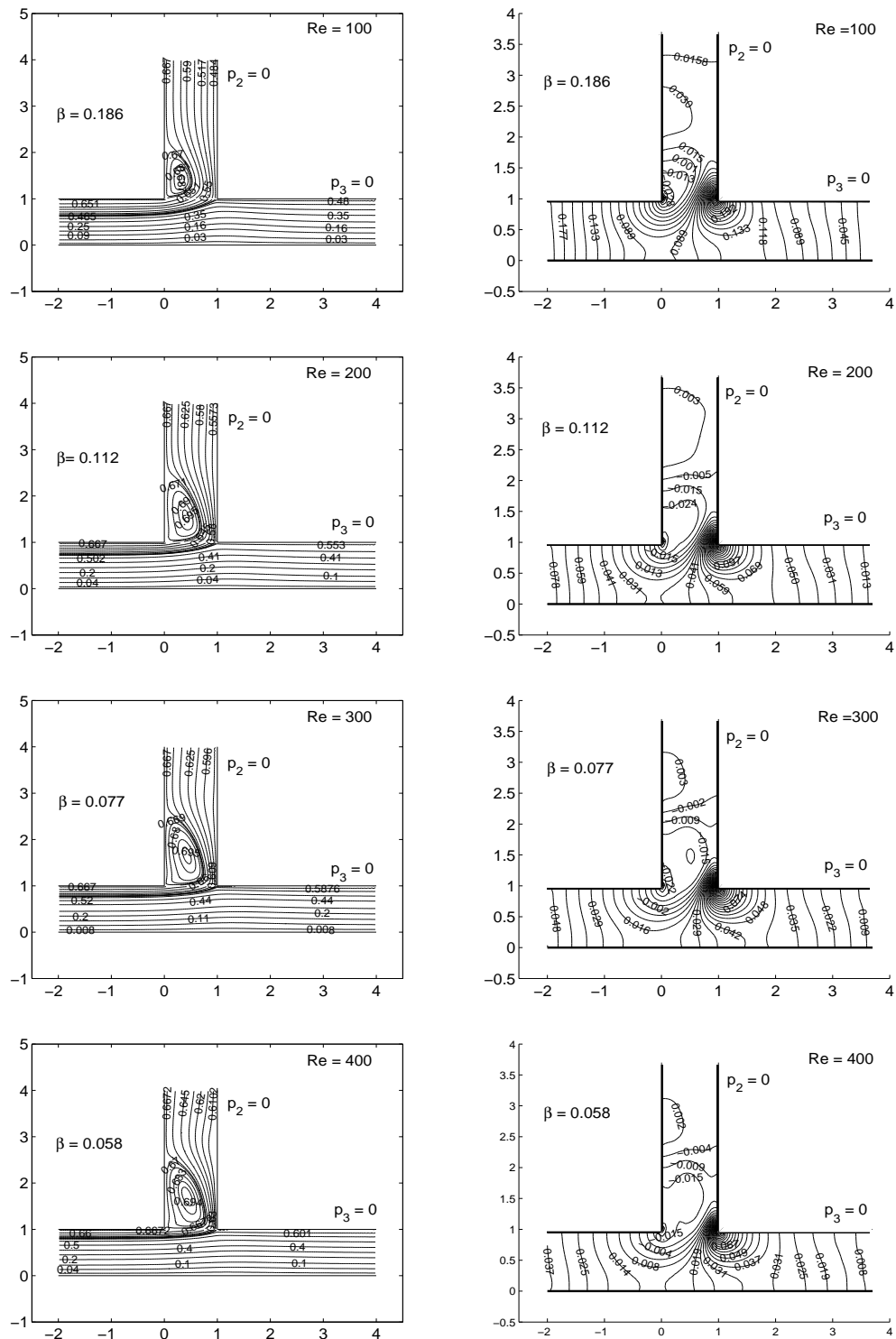


Figure 4.3 Streamline patterns and pressure contour of flow in the T-junction for various Re , and equal static pressure at the exists Γ_2^1 and Γ_3^1 .

the Reynolds number defined by bulk velocity, Re_Q and the Reynolds number defined by centerline velocity, Re_c , is $Re_c = \rho U_c w / \mu = 3Re_Q / 2$.

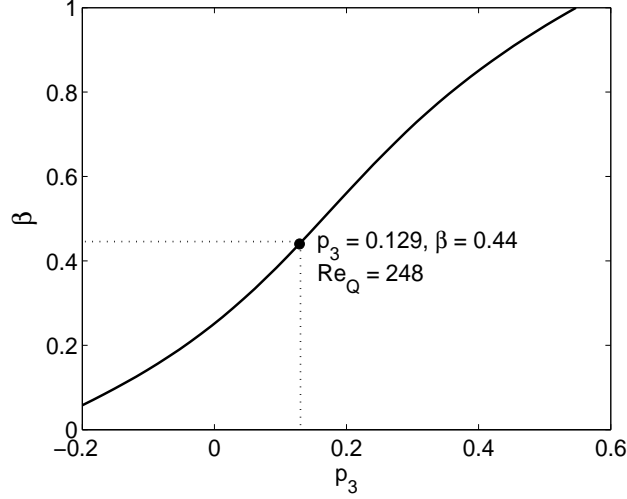


Figure 4.4 The relation between p_3 and β for $Re_Q = 248$

In our numerical experiments the computational domain was set to have lengths $L_2/w = L_3/w = 12$, whereas for the inlet duct $L_1/w = 2$. The flowing through problem T1 with fully developed parabolic velocity profile $u_x = 4(y - y^2)$, $p_2 = 0$, and various p_3 is considered. This velocity profile corresponds to non-dimensional variables where centerline velocity is used as a scale of velocity vector. To perform comparison with experiments of Liepsch *et al.* (1982) and numerical calculations of Miranda *et al.* (2008), we have to find value of p_3 , those corresponds to the flow rate ratio $\beta = 0.44$. The relation between β and p_3 is shown in Figure 4.4 for $Re_c = 372$ ($Re_Q = 248$). From results of serial computations represented by Figure 4.4, we found that $\beta = 0.44$ corresponds to the value $p_3 = 0.129$. An assessment of the mesh influence on relation between β and p_3 can be observed in Table 4.2, which lists total mass flow rate, mass flow rate through upper branch and β for three refined grids, for $Re_c = 372$ and $p_3 = 0.129$.

Figure 4.5 shows comparison of velocity profiles with experimental and numerical results represented in Miranda *et al.* (2008). Velocity profiles compared well

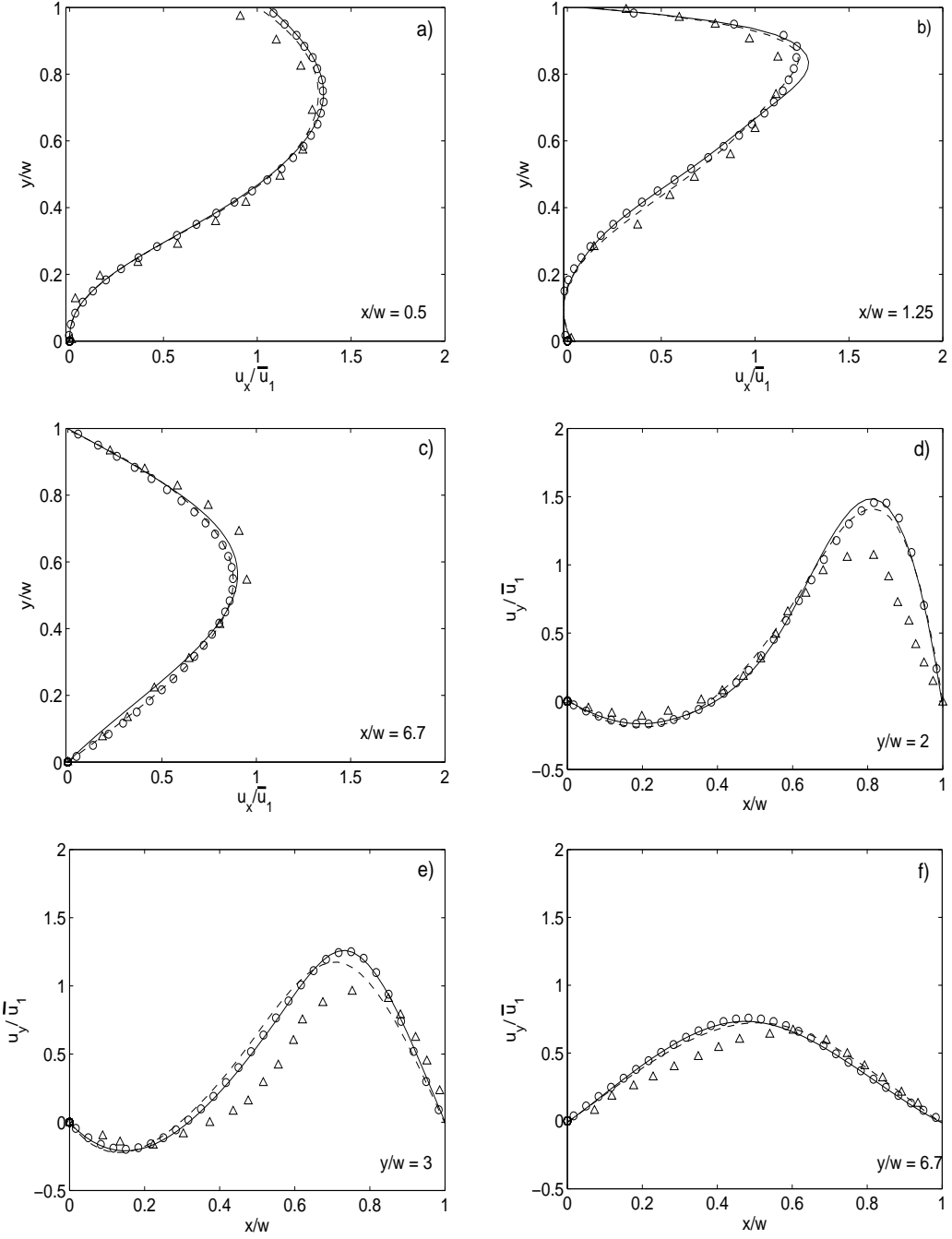


Figure 4.5 Comparison between experimental data of Liesch *et al.* (1982) and numerical data of Miranda *et al.* (2008) ($Re_Q = 248$ and $\beta = 0.44$).

Mesh	Total mass flow rate	Upper branch mass flow rate	Flow slit, β
$h_1 = 1/20$	0.670	0.294	0.438
$h_2 = 1/30$	0.668	0.293	0.439
$h_3 = 1/40$	0.667	0.293	0.439

Table 4.2 Flow split in upper branch for $Re_Q = 248$ and $p_3 = 0.129$.

with numerical results of Miranda *et al.* (2008) which are shown by solid and dashed lines. Triangle signs (Δ) are used to represent experimental data of Liepsch *et al.* (1982). Circle signs (\circ) are chosen to represent our computational results. Everywhere within the main channel the predictions of Miranda *et al.* (2008) and our results are in excellent agreements with each other and with the experimental data of Liepsch *et al.* (1982) (see Figures 4.5 a), b), and c)). The measurements indicate the existence of a separation bubble along the outer wall of the main channel (Zone $X_R = (x_r - x_s)/w$) which is accurately captured by Miranda *et al.* (2008) and our calculations (see Figures 4.5 a) and b)). However, in the branch channel the two-dimensional numerical prediction appears to consistently over predict the velocities within Zone Y_R (profiles in Figure 4.5 d) and e)). They also predict that the flow becomes fully-developed in the downstream region earlier than the measurements would indicate (profiles in Figure 4.5 f)). These discrepancies are substantially reduced by accounting for the side solid boundaries in the three-dimensional simulation, which implies that the flow at the plane of symmetry near the entrance of the branch channel is influenced by three-dimensional effects. Table 4.3 lists values of the lengths of two separation regions, X_R and Y_R , for three refined grids with $h_1 = 1/20$, $h_2 = 1/30$, and $h_3 = 1/40$. Benchmark data of Miranda *et al.* (2008) are represented in the second column of Table 4.3. The quantitative results in terms of vortex regions data for the steady flow in T-junction for $Re_c = 372$ ($Re_Q = 248$) are listed in Table 4.4.

Mesh	Miranda (2008)	$h_1 = 1/20$	$h_2 = 1/30$	$h_3 = 1/40$
X_R	2.3324	2.3275	2.3851	2.3858
Y_R	3.8878	3.7636	3.8329	3.8330

Table 4.3 X_R and Y_R for $Re_Q = 248$ and $\beta = 0.44$.

In the branch duct, the flow separates almost immediately after the upstream inlet corner ($y_s/w \approx 1.0167 - 1.022$), increase in recirculation length, Y_R , with β number increase up to $\beta \approx 0.7$, and Y_R decrease about 1% for β increase from 0.7 to 0.9, as can be verified in Table 4.4. On the other hand, for the second recirculation region attached to the lower horizontal wall, not only reattachment point, x_r , moves further downstream with β increase from 0.3 to 0.7 but also the separation point, x_s moves upstream, both contributing to increase an in recirculation length, X_R . The separation point, x_s always moves upstream with increasing values of β , whereas the reattachment location, x_r moves downstream for values of β up to 0.6 and then move backwards, in the upstream direction, for values of $\beta > 0.6$. The consequence is an increase in X_R for $\beta < 0.7$, followed by a decrease in X_R for $\beta > 0.7$. Figure 4.6 shows the developing of Main and secondary recirculation zone as a function of β when the value of β increase from 0.2 to 1.044 for $Re_Q = 248$. Figure 4.6 f) show case of $\beta = 1$, the right branch of T-junctions is closed by the recirculation zone. When $1 < \beta < 1.044$, the recirculation zone in the main branch move up to the upper wall of the right branch (see Figure 4.6 g) and h)) after that the recirculation zone in the main branch disappear (see Figure 4.6 i)). There is no numerical and experimental results to validate algorithm for flowing-through problems T2, T3, and T4. We used solution of problem T1 to generate test solution for problems T2, T3, and T4. The values of total pressure or pressure on through-flow parts was specified by the numerical solution of flowing through problem T1. Steady state solution of problems T2, T3, and T4 well compared with generating solution of problem T1.

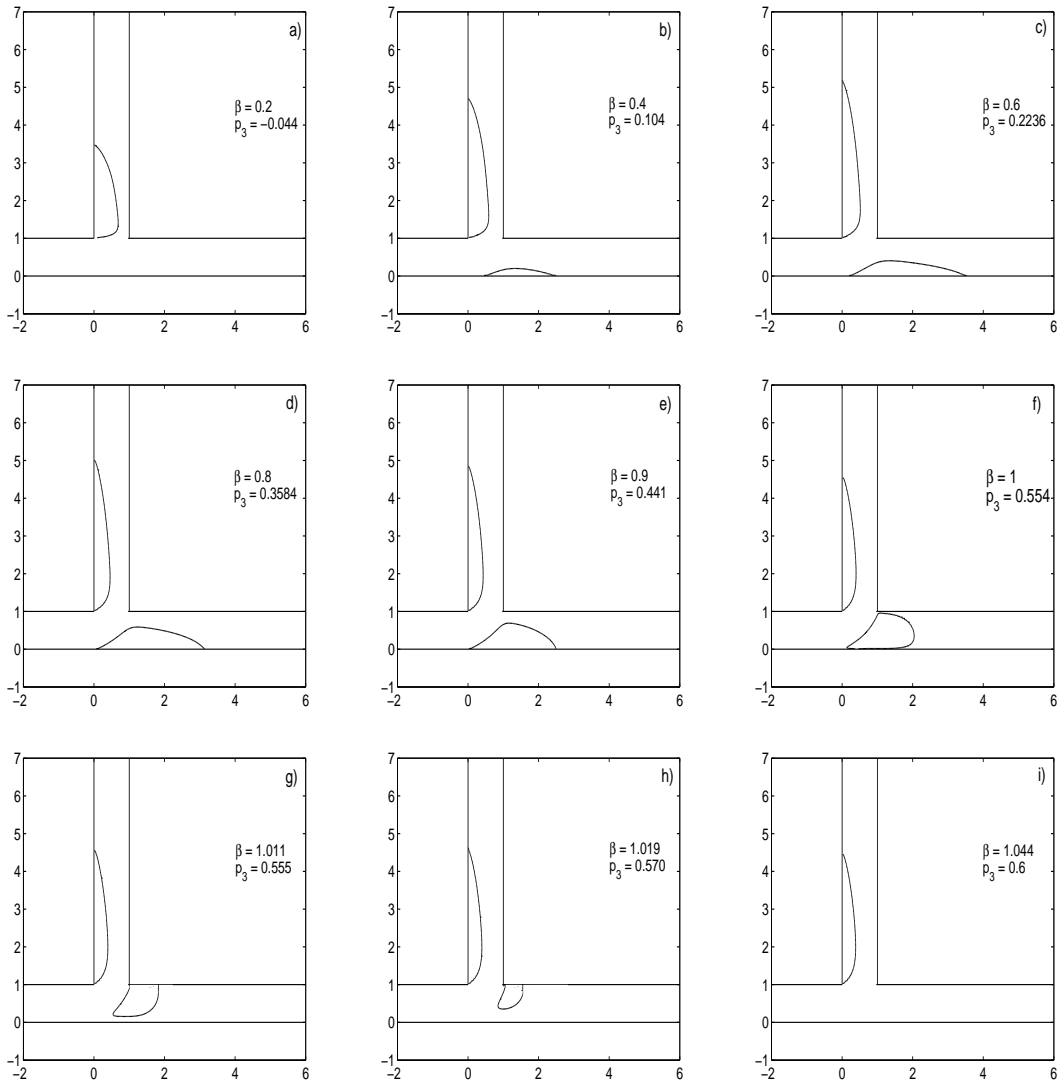


Figure 4.6 Developing of Main and secondary recirculation zone as a function of flow split β .

Flow split, β	x_s/w	x_r/w	X_R	y_s/w	y_r/w	Y_R
$\beta = 0.1$	-	-	-	1.0167	2.7056	1.6889
$\beta = 0.2$	-	-	-	1.0167	3.4692	2.4525
$\beta = 0.3$	0.7221	1.7915	1.0694	1.0167	4.1583	3.1416
$\beta = 0.4$	0.4532	2.4962	2.0430	1.0167	4.7051	3.6884
$\beta = 0.5$	0.3018	3.1260	2.8242	1.0167	4.9749	3.9582
$\beta = 0.6$	0.1976	3.5310	3.3334	1.0177	5.1210	4.1033
$\beta = 0.7$	0.1230	3.5212	3.3982	1.0189	5.1799	4.1610
$\beta = 0.8$	0.0660	3.1314	3.0654	1.0202	5.1008	3.8988
$\beta = 0.9$	0.0226	2.4978	2.4752	1.0222	4.8327	3.8105

Table 4.4 X_R and Y_R for $Re_Q = 248$.

All extensive comparisons of the computed solutions with other experimental and numerical results clearly demonstrated the good spatial resolution of proposed method and its ability to predict viscous incompressible flow in the domain with pressure(/or total pressure) specified on inflow and outflow boundaries. Above results demonstrate ability of developed numerical method to predict complex laminar flow through bounded domain with pressure (/or total pressure) specified at through-flow parts.

4.2 Flow driven by pressure differences in a 90° planar T-junctions

In this part, we illustrate the applicability of the developed numerical method to predict laminar flow driven by pressure difference. The flowing through problem with pressure and tangent component of velocity vector given on through-flow parts Γ_1^1 , Γ_2^1 , and Γ_3^1 of T-junction is well-posed (see for example Ragulin (1976), Antont-

sev *et al.* (1990)). This problem has a physical meaning. The physical situation consists of a T-junction channel connected to the three reservoirs with different level of fluid. One has to find the flow direction and volume rate through each branches of T-junction, as well as the pattern of flow in the separation region. A schematic representation of the T-branch channel along with relevant nomenclature is shown in Figure 4.1. To use advantage of symmetry, the sizes of T-junction branches are chosen the same $L_1/w = L_2/w = L_3/w = 3$. The Navier-Stokes equation is reduced to non-dimensional form with width w , as characteristic length, the dynamic velocity ν/w as the characteristic velocity, and $\rho(\nu/w)^2$ as the scale of pressure. Without loss of generality one assumes that pressure at through-flow boundary Γ_2^1 is equal to zero. No-slip boundary conditions are given on solid walls of T-junction. The following boundary conditions are prescribed on the through-flow parts (problem T1 is considered)

$$\vec{u} \cdot \vec{\tau} = u_y = 0, \quad p = p_1, \quad (x, y) \in \Gamma_1^1, \quad (4.12)$$

$$\vec{u} \cdot \vec{\tau} = u_x = 0, \quad p = 0, \quad (x, y) \in \Gamma_2^1, \quad (4.13)$$

$$\vec{u} \cdot \vec{\tau} = u_y = 0, \quad p = p_3, \quad (x, y) \in \Gamma_3^1, \quad (4.14)$$

where $p_i = (p_i^d w^2)/(\rho \nu^2)$, $i = 1, 3$ are the dimensionless pressure (superscript “ d ” denote dimensional quantity).

A schematic diagram of flow regime on the $p_1 - p_3$ plane are symbolized in Figure 4.7. Due to the symmetry ($L_1 = L_2 = L_3$), we have studied flow pattern only for $p_1 \leq p_3$. Each studied cases start from motionless state. A steady flow achieved at condition

$$\|\vec{u}^{n+1} - \vec{u}^n\| \leq \varepsilon = 10^{-8}. \quad (4.15)$$

Let us define the split number β_{ij} as the ratio of flow rate through branch i to the flow rate through branch j

$$\beta_{ij} = Q_i/Q_j, \quad Q_i = \int_{\Gamma_i^1} \vec{u} \cdot \vec{n} \, ds, \quad i, j = 1, 2, 3, \quad (4.16)$$

where \vec{n} is outward normal to through-flow part Γ_i^1 . Flow rate is positive if fluid leaves the domain and negative if fluid enters domain. To compare the numerical results with similar research, the Reynolds number, Re_i based on the flow rate Q_i is computed as steady state was reached with given p_1 and p_3 . As shown in Figure 4.7, six flow patterns exist over the range of $-5000 < p_1, p_3 < 5000$. They are denoted by the Roman numbers from I to VI. Regime I is the impacting T-junction. Laminar flow enters the T-junction through the region Γ_2 . At the junction region Γ_4 , the inlet flow stream divides into two outlet streams through regions Γ_1 and Γ_3 . Regime II corresponds to the case where fluid enters the T-junction through the region Γ_1 and Γ_2 . At the junction region Γ_4 these inlet streams merge and leave T-junction through region Γ_3 . Regime III denotes the flow pattern in which fluid enters T-junction through boundary Γ_1^1 , separates in junction region Γ_4 and leaves domain through through-flow parts Γ_2^1 and Γ_3^1 . Regime IV represents the case in which fluid enters through boundaries Γ_1^1 and Γ_3^1 , merge in Γ_4 and leaves the domain through Γ_2^1 . Regimes V and VI are symmetric with respect to the line GA to the Regimes III and II, respectively. Dashed lines in Figure 4.7 indicate equal volume flow rate through two inlets or outlets sections. Along solid lines OB , OD , and OF , flow changes pattern (or there is zero volume flow rate through some branch of T-junction). For example, there exist flow pattern III in the region between lines OB and OD . Along line OG split number $\beta_{12} = -0.5$. The streamlines and pressure contours of several particular cases are shown in Figures 4.8 a) - f) for $p_1 = p_3$. In the $p_1 - p_3$ plane, cross signs (\times) are point out to these cases. In Figures 4.8 a) - c), an arbitrary step between different streamlines were used in order to illustrate the main features of the flow field. In Figures 4.8 d) - f), an arbitrary steps between pressure contours were used in order to illustrate the main features of the pressure field. Figure 4.8 shows the case of impacting T-junction, Regime I, for $\beta_{12} = \beta_{32} = -0.5$. A recirculation zone can be seen in the top part of outlet regions Γ_1 and Γ_3 . These results demonstrate

the effect of Re_2 . The size of recirculation zone increase as Re_2 increases. A large pressure gradient is observed near stagnation point in region Γ_4 . There is a pressure gradient opposite to the flow direction along the walls in regions Γ_1 and Γ_3 where recirculations occur (see Figures 4.8 c) and f)). Figure 4.9 shows the streamline and pressure contours for the cases pointed by the triangle signs (Δ) on line OC in Figure 4.7. Regime III for equal flow rate $\beta_{21} = \beta_{31} = -0.5$ and different p_1 and p_3 are represented in Figure 4.9. The main flow from inlet region Γ_1 divides so that half portion enters the branch Γ_2 and the remainder half continuing downstream in the region Γ_3 . For $Re_1 = 91.25$, small second recirculation zone observes along lower horizontal wall of the Γ_3 region. The size of main recirculation zone along boundary $x = 0$ of Γ_2 region increase with Re_1 number increase. A large pressure gradient is observed near the right junction corners, and positive pressure gradient exist along the walls where recirculation occurs (see Figures 4.9 d) and f)). It is important to analyze the flow structure near the lines OF , OD , and OB where the fluid flow switch regime. For example, from the left hand side of curve OF in Figure 4.7, one observes Regime I, from the right hand side, one observes Regime II. Figure 4.10 shows streamlines pattern and pressure contours near line OF . In the $p_1 - p_3$ plane (Figure 4.7) signs (\square) are used to point these drawing. The recirculation zone in the region Γ_1 blocks the passage of the fluid into the branch Γ_1 (see Figure 4.10 b)). Figure 4.10 a) shows the flow of the Regime I for $\beta_{12} = -0.012$ and $\beta_{32} = -0.988$. Small amount amount of fluid enters into branch Γ_1 through narrow gap between recirculation zone and lower wall $y = 0$ of T-junction. Figure 4.10 c) shows the case of flow belonging to Regime II for $\beta_{12} = 0.005$ and $\beta_{32} = -1.005$. Now fluid enter into region Γ_4 through gap near left corner of T-junction. The large pressure gradient exist near right corner of T-junction (see Figures 4.10 d), e), and f)). There is opposite to the flow direction pressure gradient along the upper wall of branch Γ_3 . This gradient is located in the region of recirculation zone near right corner

of T-junction along the solid boundary. Figure 4.11 shows streamlines pattern and pressure contours near line OD . The down triangular signs (∇) denote these cases in Figure 4.7 in the $p_1 - p_3$ plane. Figure 4.11 b) corresponds to the case $\beta_{21} = 0$ (zero flow rate through boundary Γ_2^1). Recirculation zone closes branch Γ_2 for fluid flow. Figure 4.11 a) represents stream line pattern for the Regime II for $\beta_{21} = 0.003$ and $\beta_{31} = -1.003$. Flow stream from Γ_2 merge the main stream between Γ_1^1 and Γ_3^1 through small gap near left corner of T-junction. Flow of Regime III is shown in Figure 4.11 c) for $\beta_{21} = -0.003$ and $\beta_{31} = -0.997$. Fluid enters into the branch Γ_2 through small gap between recirculation zone and right corner of side branch. The secondary recirculation zone along wall $y = 0$ was not observe in these cases. The large pressure gradient exists near right corner of junction (see Figures 4.11 d) - f)). Constant pressure gradient in branch Γ_1 and Γ_3 generates the main stream. In the region Γ_4 small disturbance of pressure fields is happen due to the presence of upper branch Γ_2 . Figure 4.12 demonstrates the streamlines pattern and pressure contours for the range of parameter where transection between Regimes III and IV observes. These case mark by \bigcirc circle signs in Figure 4.7. Figure 4.12 b) shows case of $\beta_{31} = 0$ and $\beta_{21} = -1$. The right branch Γ_3 is closed by recirculation zone. The pattern of stream line very similar to the pattern demonstrate in Figure 4.10 b). Flow corresponding to Regime IV is depicted in Figure 4.12 a) and d). Small amount of fluid merge the main stream along wall $y = 0$. Flow pattern of Regime III for $\beta_{21} = -0.994$ and $\beta_{31} = -0.006$ is represented by Figure 4.12 c) and f). Small amount of fluid enters in to region Γ_2 through the small gap between right corner of the junction and recirculation zone which adjoints wall $y = 0$. Significantly large pressure gradient observe near left corner of junction (see Figures 4.12 d) - f)). There is opposite to the flow direction pressure gradient along wall $x = 0$ in the Γ_2 region (see Figures 4.12 d) - f)). This pressure gradient responsible for recirculation zone near this corner.

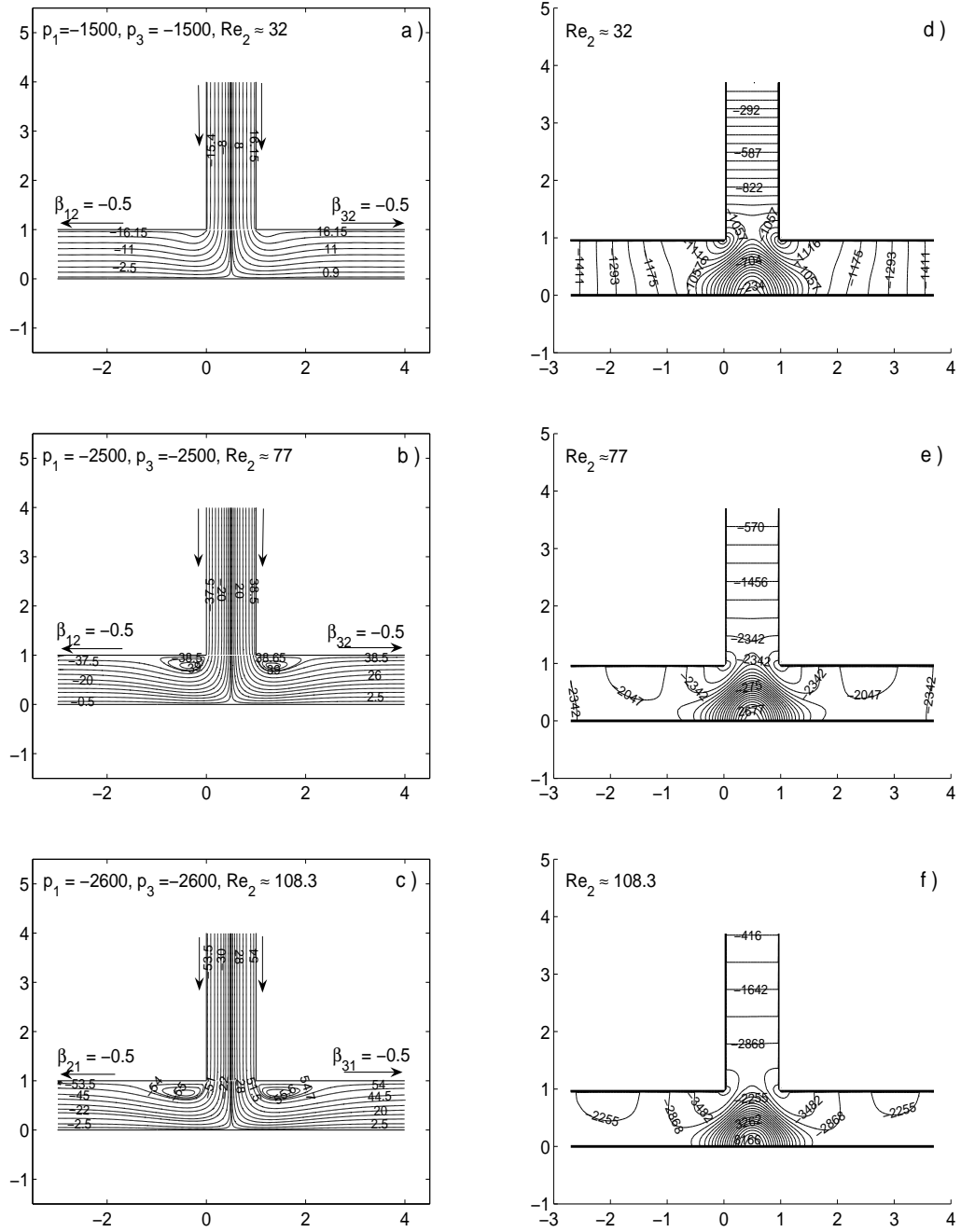


Figure 4.8 The streamline (left column) and pressure contours (right column) for impacting T-junction. See cross signs (\times) on line OG in Figure 4.7.

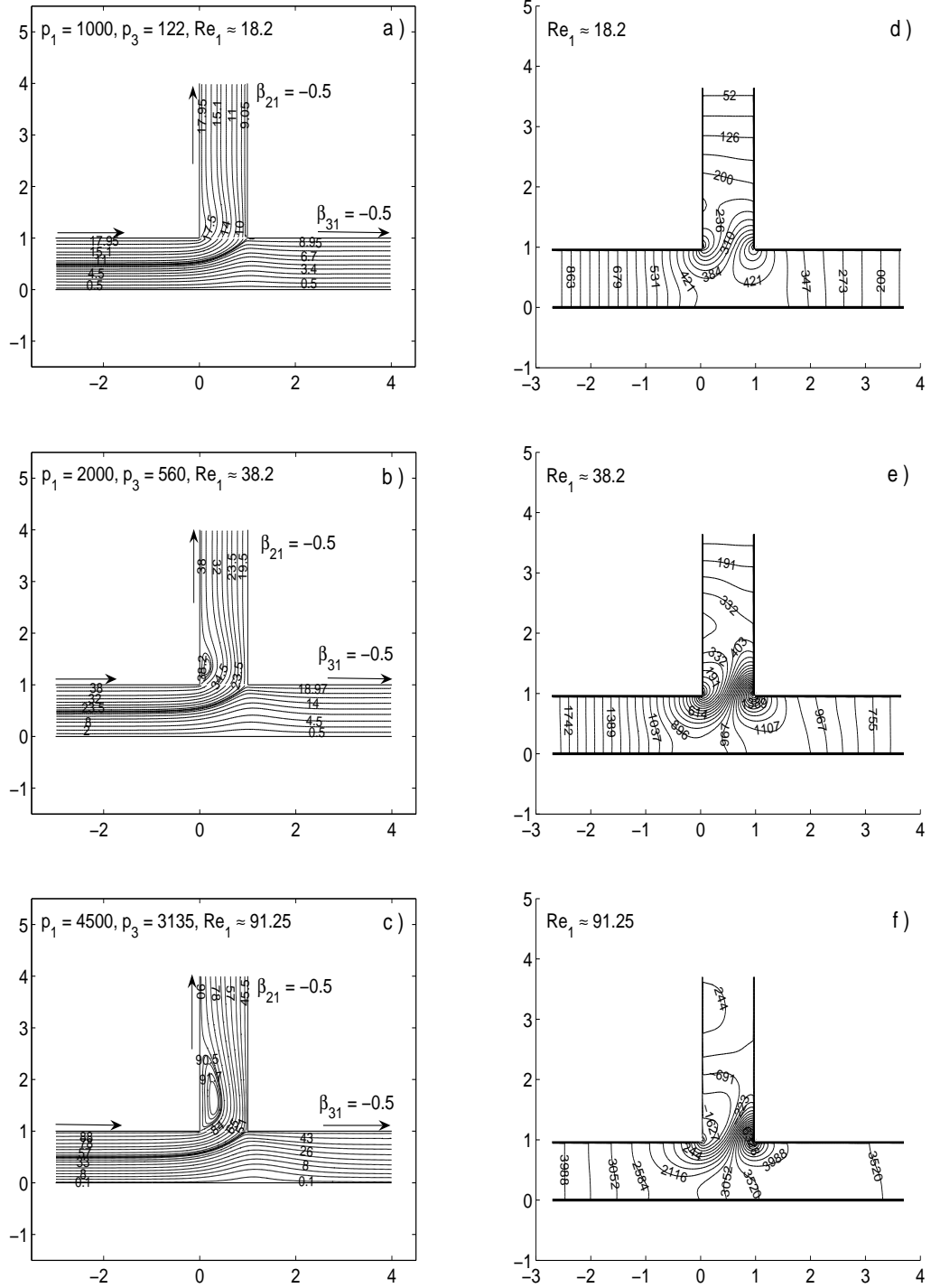
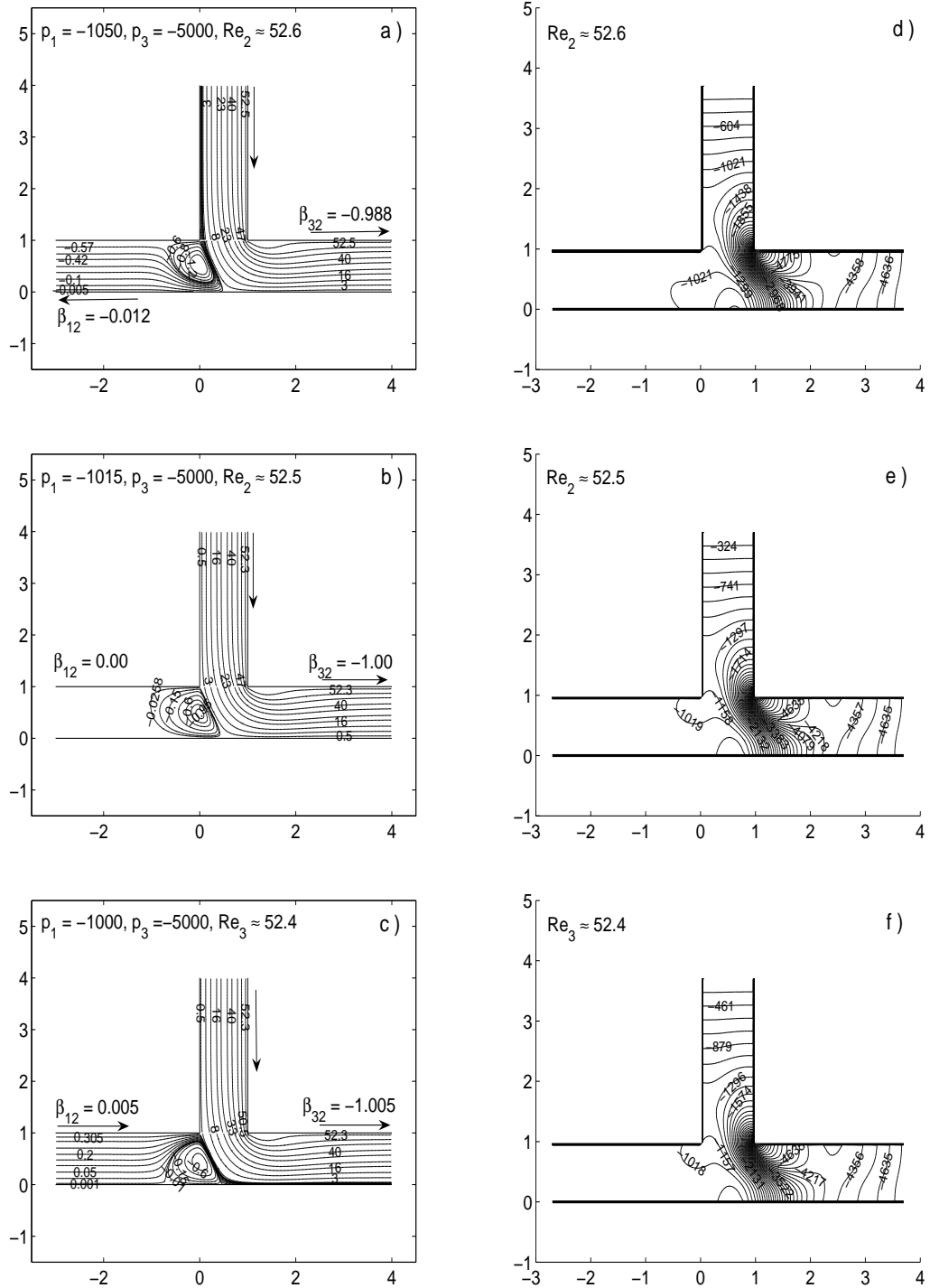
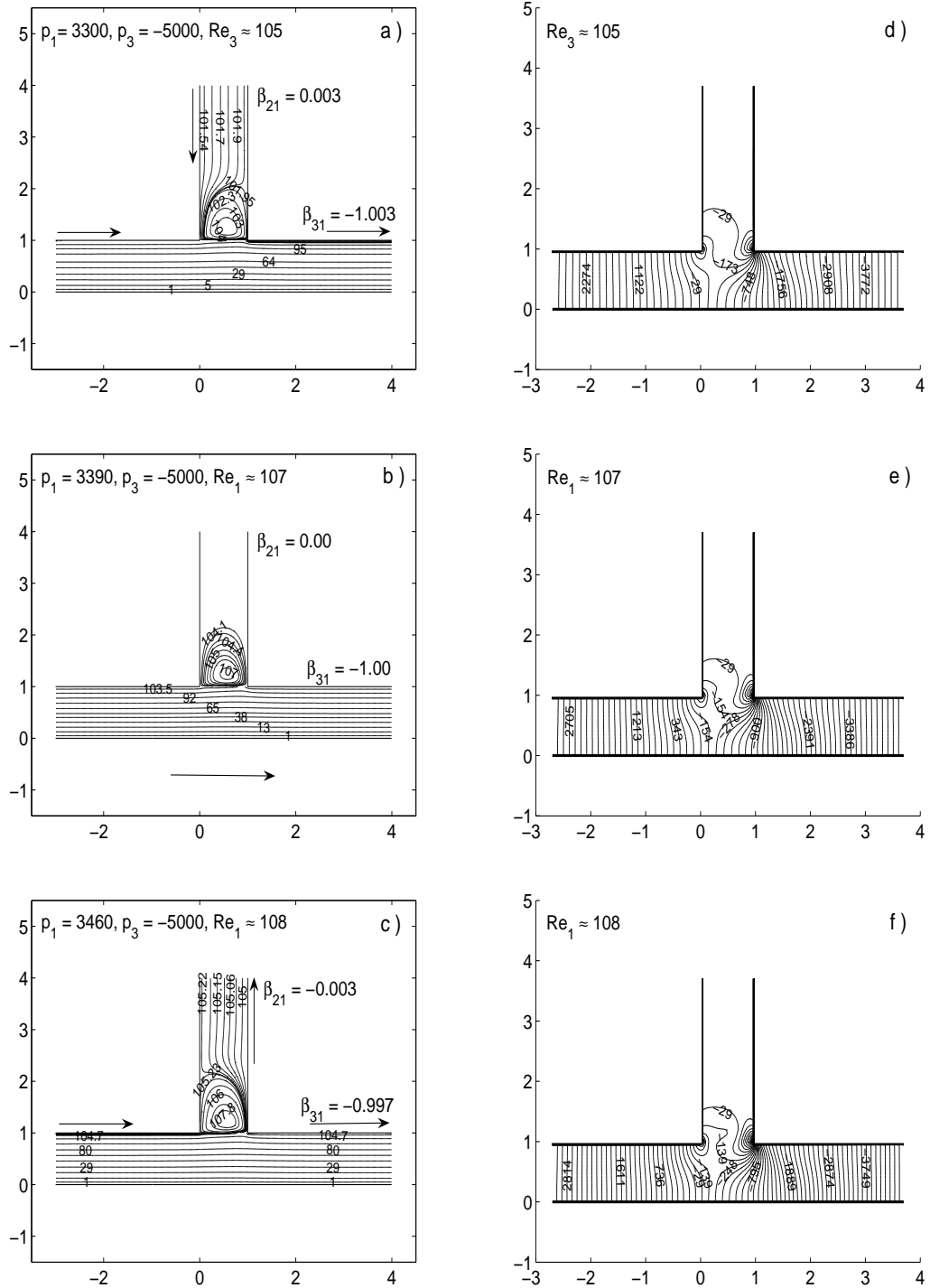


Figure 4.9 The streamline (left column) and pressure contours (right column) for the case correspond to triangle signs (Δ) on line OC in Figure 4.7.





CHAPTER V

FLOW IN U-BEND CHANNEL

This chapter is concerned with the application of the developed in previous chapter, numerical method to simulate steady and unsteady laminar flow in a planar 180° bend (U-bend). The two-dimensionality assumption adopted can be justify due to the high geometrical aspect ratios occurring in the practical applications.

Flow in curved tube and serpentine flow channels are encountered in a wide variety of applications, for example, air conditioning and refrigeration systems, chemical reactors, food and dairy process. In this study, the flow in U-bend channel is considered as flowing through problem for viscous incompressible flow. Varied of boundary condition of through-flow parts have been studied. To the best of the authors knowledge, there are no experimental data for two-dimensional laminar flows in U-bend channel. Consequently, the present numerical results can not be compared directly with measurements. Instead, the validation of numerical algorithm has been performed on grid sequence and by comparing different type of boundary conditions considered in Chapter II

5.1 Steady flow in U-bend channel

We consider a fully developed laminar flow through a 180° U-bend channel. The flow configuration, the coordinate system and the main notations are shown in Figure 5.1. Let d be the width of channel. Let the radius of curvature of the centerline of channel be R . The length L of channel before and after the bend are taken sufficiently large to assume that pressure at sections $A_1A'_1$ and $A_2A'_2$ can be considered as constant and fluid enters or leaves the channels legs with laminar,

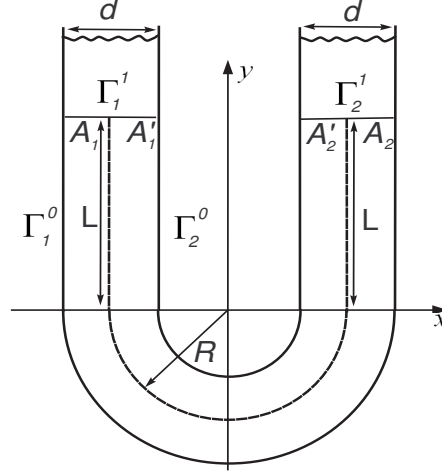


Figure 5.1 Schematic diagram of U-bend channel.

fully developed velocity profile. The flow structure depends on two non-dimensional parameters, the curvature ratio $\delta = R/d$ and Reynolds number $Re = Ud/\nu$, where U is the mean velocity and ν is the kinematic viscosity. The developed finite volume method has been utilized to simulate steady flow. Three kinds of the flowing through problem have been considered. In all cases no-slip boundary conditions hold in impermeable parts Γ_1^0 and Γ_2^0 . The three flowing through problems are formulated by the following:

- **U1.** On through-flow parts Γ_1^1 , tangent and normal components of velocity vector are given

$$\vec{u} = (u_x, u_y) = (0, u_s^1(x)), \quad \vec{x} \in \Gamma_1^1,$$

where $u_s^1(x)$ is the parabolic Poiseuille velocity profile. On through-flow parts Γ_2^1 , tangent component of velocity vector and pressure are specified

$$\vec{u} \cdot \vec{\tau} = u_x = 0, \quad p = p_2, \quad \vec{x} \in \Gamma_2^1.$$

- **U2.** On through-flow parts Γ_1^1 and Γ_2^1 , tangent component of velocity vector and pressure are specified

$$\vec{u} \cdot \vec{\tau} = u_x = 0, \quad p = p_1, \quad \vec{x} \in \Gamma_1^1,$$

$$\vec{u} \cdot \vec{\tau} = u_x = 0, \quad p = p_2, \quad \vec{x} \in \Gamma_2^1,$$

where $\vec{\tau}$ is unit tangent vector to Γ_1^1 and Γ_2^1 and $p_1 > p_2$.

- **U3.** On through-flow parts Γ_1^1 , tangent component of velocity vector and total pressure are prescribed

$$\vec{u} \cdot \vec{\tau} = u_x = 0, \quad p + \frac{1}{2}\rho|\vec{u}^2| = H_1(\vec{x}), \quad \vec{x} \in \Gamma_1^1,$$

where $H_1(\vec{x})$ is given function and prescribed with solution of U1. On through-flow parts Γ_2^1 , tangent component of velocity vector and pressure are known (see equation (2.6))

$$\vec{u} \cdot \vec{\tau} = u_x = 0, \quad p = p_2, \quad \vec{x} \in \Gamma_2^1.$$

The main characteristic of flow in curve channels is pressure losses. Due to the extensive use of curve of pipe in industry, knowledge about the pressure losses, flow patterns, and other characteristics are very important. Pressure losses characteristics are required for evaluating pump power required to overcome pressure losses to provide the necessary flow rates. The pressure losses are also functions of the curvature of the tube. The pressure losses are presented in a form of Darcy friction factor (Popiel and Wojtkowiak, 2000) versus Reynolds number

$$f_w = \frac{2\Delta p}{\rho U^2 \frac{L}{d}} = f(Re)$$

where Δp is the pressure losses, $\Delta p = p_2 - p_1$.

Before the main computations were started, a test was executed with the straight channel. A very good agreement of the computed pressure losses with the theoretical solution based on the Poiseuille law $f_w = 36/Re$ was observed. Based on the preliminary experiments, the length of the channel legs, $L/d = 5$, have been used in the main computation represented below. The impermeable boundaries A_1A_2 and $A'_1A'_2$ equally partitioned on M subintervals. The flowing through parts $A_1A'_1$ and

Grid	Darcy friction factor, f_w		
	U 1	U 2	U 3
100x10	0.431543	0.431238	0.431782
200X20	0.429796	0.429743	0.429832
4000X40	0.429668	0.429647	0.429701
order	1.936337	2.025377	1.994849

Table 5.1 Darcy friction for three kinds of the flowing through problem, $Re = 100, \delta = 3$.

$A_2A'_2$ divided on equal number of N subintervals. Three grids sequence of 100×10 , 200×20 , and 400×40 nodes were tested. Results of computations on grids sequence are shown in Table 5.1 in terms of f_w for $Re = 100$ and $\delta = 3$. In the problem U1, Reynolds number is known a priori and Δp was estimated from the steady state flow regime. In the case of flowing through problem U2 the pressure losses is known a priori and Reynolds number was computed from the steady state flow rate. In the problem U3, neither Δp or Re is known a priori and both of them compute at the end of the numerical simulation from steady state.

Pressure losses of a U-bend channel flow are presented in a form of the Darcy friction factor versus Reynolds number $f_w = f(Re)$ in Figure 5.2, where the effect of the dimensionless curvature ratio, $\delta = R/d$, is shown as well. All three flowing through problems U1, U2, and U3 give very close results. From Figure 5.2, it is seen that the effect of the channel curvature ratio on the friction factor is small for $\delta > 3$ for all three tested flowing through problems. The Darcy factor, f_w , increase with δ decrease. In Figure 5.3 streamline patterns are presented. Figure 5.3(a) is drawn for $\delta = 1, Re = 200$, Figure 5.3(b) is drawn for $\delta = 1, Re = 300$, Figure 5.3(c) is drawn for $\delta = 0.6, Re = 200$, and Figure 5.3(d) is drawn for $\delta = 0.6, Re = 300$. The sharp bend $\delta = 0.6$ and increasing Reynolds number cause separation which occurs on the

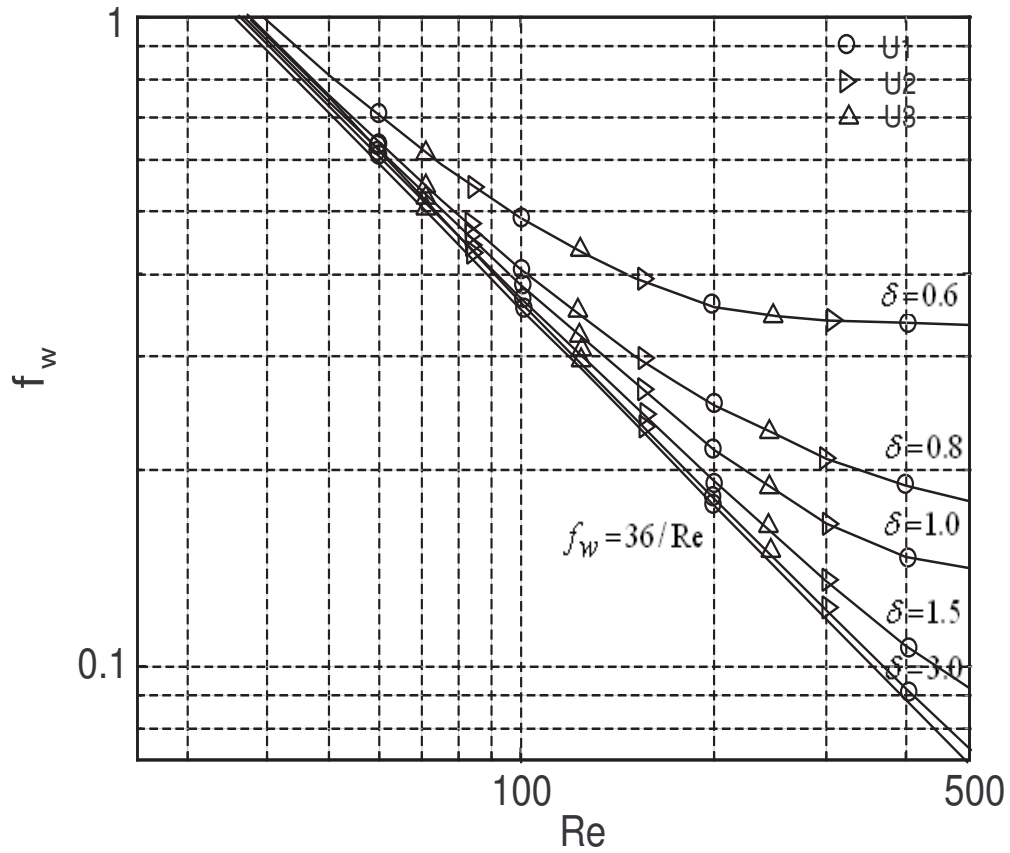


Figure 5.2 Friction factor as a function of Reynolds number.

right hand side of the bend. The size of separation zone increases with increasing of flow rate and decreasing δ .

5.2 Oscillating flow through U-bend channel

The two-dimensional oscillating flow of an incompressible viscous fluid in U-bend channel is considered. The physical situation is the followings: at instant time the level of fluid in one of the channel legs is higher than in other. The motion starts from the state of rest. The fluid performs a damped oscillatory motion. The two forces acting on the fluid columns are the resistance force and pressure force due to the unbalance weight of the fluid in legs of U-bend channel. The correct prediction of the amplitude, frequency, and damping of these oscillation is necessary for many

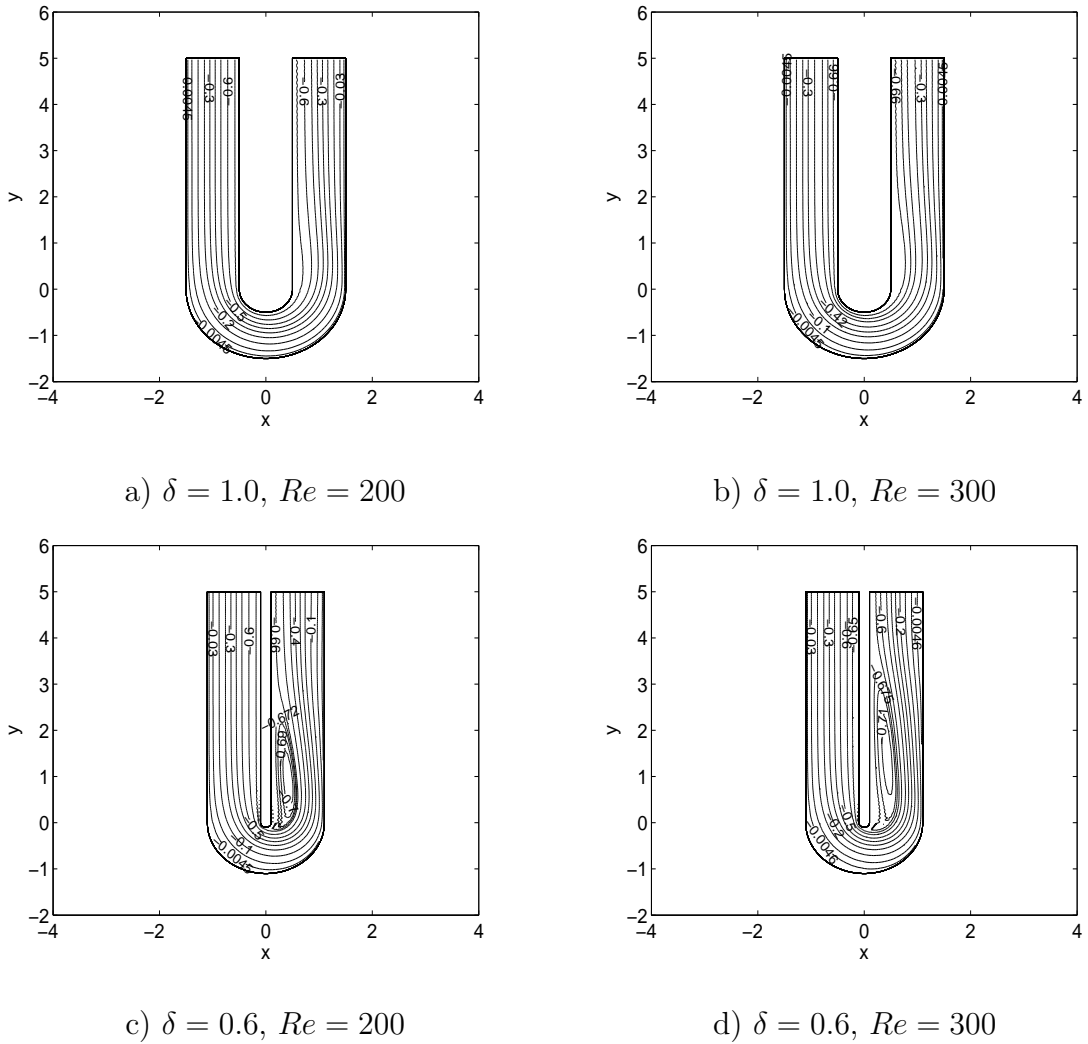


Figure 5.3 Streamline patterns of flow in the U-bend channel for various δ and Re .

technical devices. The study of frequency, amplitude, and damping factor cannot be done if velocity is given advanced on through-flow parts. By this end, we came to the boundary value problem with pressure given at through-flow parts. The flow configuration, the coordinate system, and the main notations are shown in Figure 5.4

Let d be the width of the channel. Let the radius of curvature of the centerline of the channel be R . Let the legs of channel be large enough to assume that pressure at section $A_1A'_1$ and $A_2A'_2$ depends only on simultaneous hydrostatic pressure

$$p(t) |_{A_1A'_1} = \rho g z_1(t), \quad p(t) |_{A_2A'_2} = \rho g z_2(t),$$

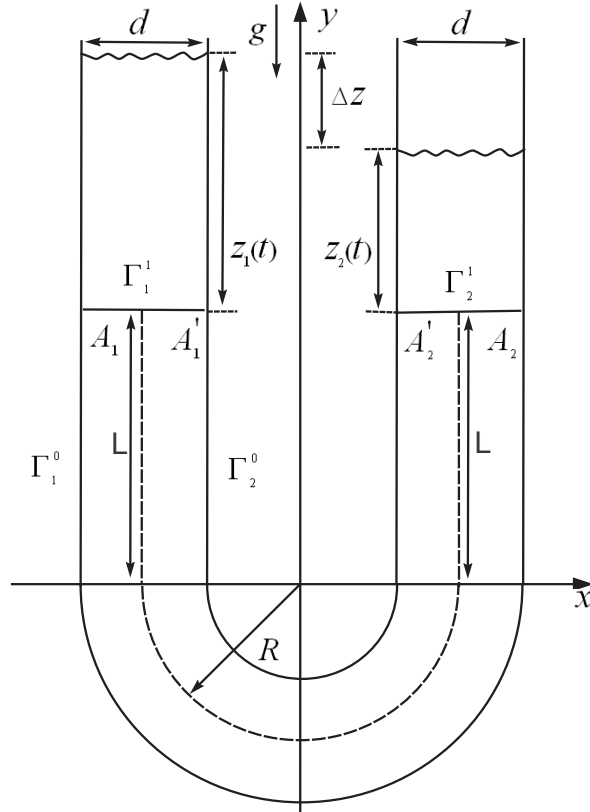


Figure 5.4 Schematic diagram of oscillating flow in U-bend channel.

where ρ is the fluid density, g is the gravity acceleration, and $z_1(t)$ and $z_2(t)$ are displacement of fluid surface from through-flow boundaries Γ_1^1 and Γ_2^1 , respectively. Surface displacements $z_1(t)$ and $z_2(t)$ satisfy to the following equations

$$\begin{aligned} z_i(t) &= z_i(0) + \frac{Q_i(t)}{d} = z_i(0) + \frac{1}{d} \int_0^t \int_{A_i} \vec{u} \cdot \vec{n} \, ds \, dt \\ &= z_i(0) + \frac{\text{Flow volume rate}}{\text{Width of channel}}, \quad i = 1, 2. \end{aligned}$$

The following initial condition are used

$$\vec{u}(x, y, 0) = 0, \quad z_i(0) = z_i^0, \quad i = 1, 2.$$

Since the flow does not have characteristic velocity, the problem is dimensionlized with d as characteristic length, the dynamic velocity ν/d as the characteristic velocity, and $\rho(\nu/d)^2$ as the scale of pressure,

$$t = \frac{d^2}{\nu} t', \quad \vec{x} = d \vec{x}', \quad \vec{u} = \frac{\nu}{d} \vec{u}', \quad p = \rho \left(\frac{\nu}{d} \right)^2 p'.$$

Because pressure in Navier-Stokes equation is determined up to arbitrary function of time, one can assume $p(t)|_{\Gamma_2^1} = 0$. With this assumption the non-dimensional flowing through problem U2 has the following form

$$\frac{\partial u_x}{\partial t} + u_x \frac{\partial u_x}{\partial x} + u_y \frac{\partial u_x}{\partial y} = -\frac{\partial p}{\partial x} + \nabla^2 u_x, \quad (5.1)$$

$$\frac{\partial u_y}{\partial t} + u_x \frac{\partial u_y}{\partial x} + u_y \frac{\partial u_y}{\partial y} = -\frac{\partial p}{\partial y} + \nabla^2 u_y, \quad (5.2)$$

$$\frac{\partial u_x}{\partial x} + \frac{\partial u_y}{\partial y} = 0, \quad (5.3)$$

where $\vec{u} = (u_x, u_y)$. Initial and boundary conditions are the following

$$\vec{u} = (u_x, u_y) = 0, \quad (x, y, t) \in \Gamma_1^0 \cup \Gamma_2^0, \quad (5.4)$$

$$\vec{u} \cdot \vec{\tau} = (u_x, 0) = 0, \quad p(x, y, t) = \frac{1}{Fr} \Delta z(t), \quad (x, y, t) \in \Gamma_1^1, \quad (5.5)$$

$$\vec{u} \cdot \vec{\tau} = (u_x, 0) = 0, \quad p(x, y, t) = 0, \quad (x, y, t) \in \Gamma_2^1, \quad (5.6)$$

$$\vec{u}(x, y, 0) = 0, \quad \Delta z(0) = \Delta z^0, \quad (5.7)$$

where $Fr = \nu^2/gd^3$ is the dimensionless parameter define ratio of inertia and gravitational forces, $\Delta z^0 = z_1(0) - z_2(0)$, and $\Delta z(t) = z_1(t) - z_2(t)$ is the displacement of fluid from the equilibrium position,

$$\Delta z(t) = \Delta z^0 + 2 \int_0^t \int_A^{A'} \vec{u} \cdot \vec{n} \, ds \, dt. \quad (5.8)$$

Because fluid flow is incompressible, the integral in (5.8) can be takes over any section of channel. The developed in Chapter III, finite volume method has been applied to simulate oscillating flow in the formulation (5.1)-(5.8)

There are three different kinds of damped oscillatory motion, which depend on curve ratio δ , and non-dimensional parameter Fr . The motion is said to be under damped if the solution oscillates at some real frequency and decays in time at a rate proportional to the damping term $Fr = \nu^2/gd^3$. The motion is said to be critically damped if the solution decays without oscillating. The motion is said to be over

damped if the solution again decays without oscillating. The motion is said to be over damped if the solution again decays without oscillating but rate of decay lower than in critical case.

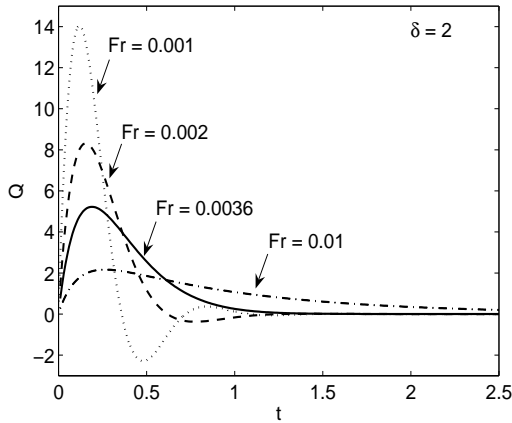


Figure 5.5 Predicted variation of volume rate with time.

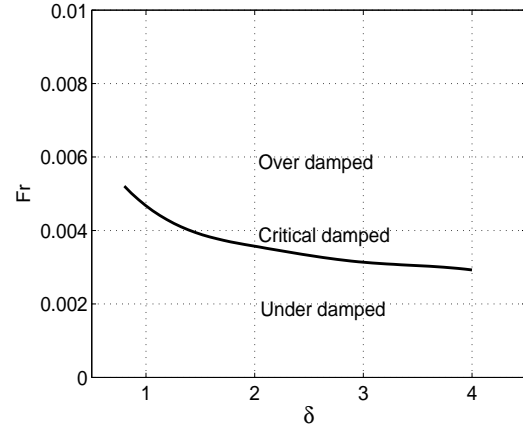


Figure 5.6 Schematic diagram of damped oscillatory motion regime.

All these three regime of fluid motion can be observed in Figure 5.5, where variations of volume rate $Q(t)$ versus time are represented for fixed curvature ratio $\delta = 2$ and $Fr = 0.001$, $Fr = 0.002$, $Fr = 0.0036$, and $Fr = 0.01$. Initial displacement is $\Delta z^0 = 5$. It can be seen from Figure 5.5 that critically damped motion corresponds to $Fr = 0.0036$ and is shown in Figure by solid line. Dash-dotted line represents over damped regime for $Fr = 0.01$. Dash line is using to demonstrate under damped motion for $Fr = 0.002$. It is clear that critically damped solution is more rapidly damped to equilibrium state than either the under damped or over damped solutions. Figure 5.6 shows diagram of oscillatory motion regime in the (δ, Fr) -plane. Solid line represents critically damped motion. There is over damped motion for parameters δ and Fr above this curve. Under damped oscillatory motion have been observed for parameters δ and Fr below solid line. In many applications, the area-average momentum balance equations are used to simulate oscillatory motion in U-bend channel. In such models, it is usually assumed that the resistance in unsteady flow is

given by steady flow resistance at the same velocity in the case of straight channel. It is understood that this assumption is a potential source of error. The effect of variable

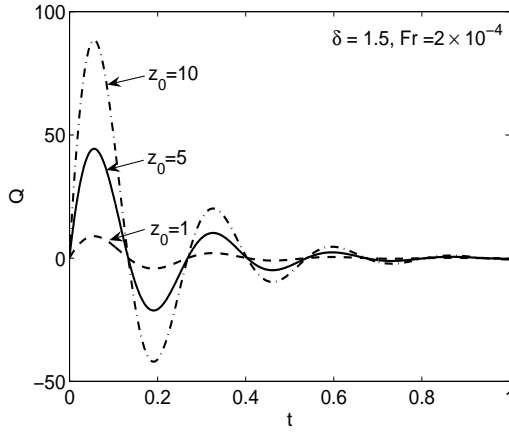


Figure 5.7 Variations of volume rate with time. Influence of initial displacement.

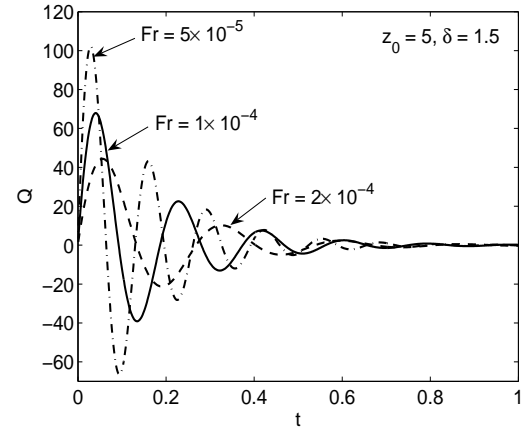


Figure 5.8 Variation of volume rate with time. Influence of Fr .

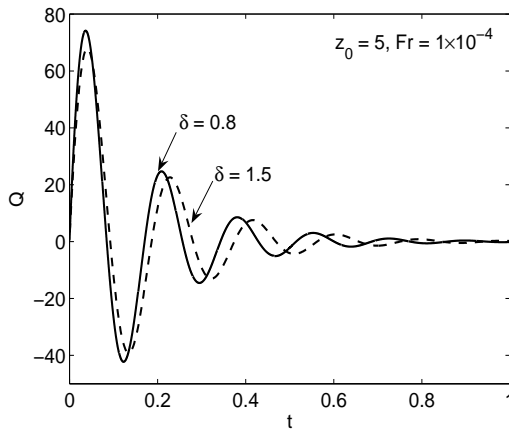


Figure 5.9 Variation of volume rate with time. Influence of curvature ratio δ .

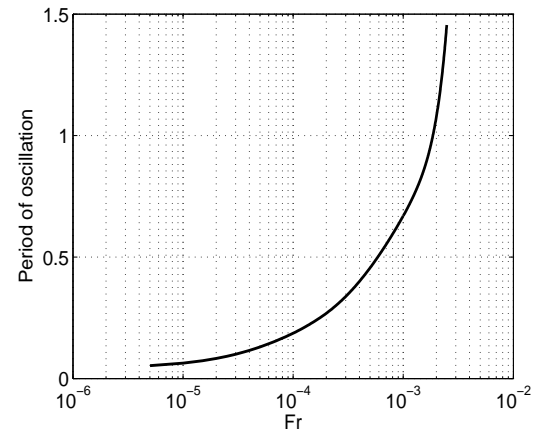


Figure 5.10 Period of oscillation with Fr .

Δz^0 , δ , and Fr on the oscillation characteristics is illustrated in Figure 5.7 - 5.10. Figure 5.7 shows influence of initial displacement of fluid columns on the oscillatory motion. This Figure is drawing for fixed value of $\delta = 1.5$ and $Fr = 2 \times 10^{-4}$. It

can be seen that period of oscillations does not depend on initial displacement. Only amplitude of oscillation is applied. The attenuation of oscillation by increasing Fr is plotted in Figure 5.8 in the form of variation of volume rate versus time for fixed $\Delta z^0 = 5$ and $\delta = 1.5$. For larger value of Fr period of oscillation increase and amplitude decrease. The effect of variation of curvature ratio δ on the oscillation is represented in Figure 5.9, for fixed $Fr = 1 \times 10^{-4}$ and $\Delta z^0 = 5$. It can be seen that the two represented cases (corresponding $\delta = 0.8$ and $\delta = 1.5$) have different periods of oscillations and different damping rate. The effect of parameter Fr on the period of oscillation is illustrated in Figure 5.10 for the case $\delta = 1.5$ and $\Delta z^0 = 5$.

CHAPTER VI

GENERAL SUMMARY AND CONCLUSIONS

6.1 General summary and conclusions

The purpose of this study was to develop and validate numerical method for solving the incompressible time-dependent Navier-Stokes equations in domain with through-flow parts where boundary condition for pressure or total pressure are given.

Several variants of flowing-through problems for incompressible viscous Navier-Stokes equation with pressure (/or total pressure) boundary condition, whose solvability is proved by Antontsev *et al.* (1990), Ragulin (1976), and Ragulin *et al.* (1980) are represented in Chapter II. A computational method for the solution of the several variants of well posed flowing through problems is developed within the frameworks of finite volume methodology on non-staggered boundary fitted quadrilateral grids and a pressure correction based solution techniques is used for time discretization. In the case of boundary conditions formulated for pressure (/or total pressure), it is necessary to satisfied an incompressibility requirement, $\nabla \cdot \vec{u} = 0$, on this part of boundary. The algorithms that we have developed was validate by simulating pressure driven flows between parallel plates and in annular between two cylinders for both of those analytical solutions are given. The results of our numerical solutions are in good agreement with analytical solutions.

The developed and validated algorithms to solution of flowing through problem was applied to simulate viscous incompressible flow in T-junction channel. Comparison of our numerical solution with known experimental and computational data for the two-dimensional flow through 90° T-junction demonstrates robustness and good

accuracy of developed code. A diagram of flow patterns depending on pressure differences between T-junction branches have been studied. The method allowed to determine direction of the flow through each branches and structure of flow pattern in junction region in case of pressure (/or total pressure) is given on through-flow parts of domain.

The numerical simulation of steady and unsteady oscillating fluid flow through U-bend channel have been conducted. Finite volume method developed to solve flowing through problem was utilized. Results of these calculations demonstrate that flowing through problem with pressure on through-flow parts of domain boundary can be effectively used to predict steady and unsteady motion of viscous incompressible fluid flows in case of complex domain geometry where it is impossible to prescribed velocity profile as boundary conditions on through-flow parts of boundary.

6.2 Contribution to knowledge

The work presented in thesis provide original contribution to the body of knowledge concerning the numerical simulation of viscous incompressible flow with pressure (/or total pressure) known on the domain boundary. The main contributions are as follows:

- Finite volume method developed and validated.
- Exact analytical solution of flow with circular streamline in annular domain between two cylindrical surface have been found.
- Variety o flow regime in T-junction channel have been analyzed depending on pressure drops between branches.
- Parametric study of naturally oscillating fluid flow through U-bend channel have been conducted.

6.3 Recommendation for future research

The work presented in this thesis provides the foundation for the numerical simulation of complex fluid and air flows in the case where on the boundary information about velocity is not available but pressure or total pressure is known. There are several areas where further research is required.

- Developed three-dimensional code.
- Analyze three-dimensional flow in T-junction with pressure (/or total pressure) given as boundary conditions.
- Study unsteady flow in the domain with more than three through-flow boundaries.

REFERENCES

REFERENCES

- Anagnostopoulos, J.S., and Mathioulakis, D.S. (2004). Unsteady flow field in a square tube T-junction. **Physics of Fluids** 16(11):3900-3910.
- Antontsev, S.N., Kazhikhov, A.V., and Monakhov, V.N. (1990). **Boundary Value Problems in Mechanics of Nonhomogeneous Fluids**. Elsevier Science Publishing Company Inc, New York.
- Chorin, A.J. (1968). Numerical solution of the Navier-Stokes equations. **Mathematics of Computation** 22(104):745-762.
- Chorin, A.J., and Marsden, J.E. (1990). **A Mathematical Introduction to Fluid Mechanics**. Springer-Verlag, New York.
- Donald, S. (1968). A two-dimensional interpolation function for irregularly-spaced data. **ACM**. 23:517-524.
- El-Shboury, A.M.F., Soliman, H.M., and Ormiston, S.J. (2003). Laminar forced convection in two-dimensional impacting tee junctions. **Heat and Mass Transfer** 39:815-824.
- Fernandez-Feria, R., and Sanmiguel-Rojas, E. (2004). An explicit projection method for solving incompressible flows driven by a pressure difference. **Computers & Fluids** 33:463-483.
- Ferziger, J.H., and Peric, M. (1996). **Computational Methods for Fluid Dynamics**. Springer, Singapore.
- Fletcher, C.A.J. (1990). **Computational Techniques for Fluid Dynamics 1**. Springer-Verlag, New York.

- Fluent Inc. (1998). **Fluent 5.0 User's Guide**. Fluent Incorporated, Lebanon.
- Hayes, R.E., Nandkumar, K., and Nasr-El-Din, H. (1989), Steady laminar flow in a 90 degree planar branch. **Computers & Fluids** 17(4):537-553.
- Heywood, J.G., Rannacher, R., and Turek, S. (1996). Artificial boundaries and flux and pressure conditions for the incompressible NavierStokes equations. **International Journal for Numerical Methods in Fluids** 22:325-352.
- Kelkar, K.M., and Choudhury, D. (2000), Numerical method for the prediction of incompressible flow and heat transfer in domains with specified pressure boundary conditions. **Numerical Heat Transfer** 38:15-36.
- Kobayashi, M.H., Pereira, J.C.F., and Sousa, J. M. M. (1993). Comparison of several open boundary numerical treatments for laminar recirculating flows. **International Journal for Numerical Methods in Fluids** 23:971-979.
- Kuznetsov, B.G., Moshkin, N.P., and Smagulov, S.h. (1983). Numerical simulation of viscous incompressible flow in channels with complicated geometry under preassigned pressure overfall. **Institute of Thermophysics, Siberian Branch of the Russian Academy of Sciences, Novosibirsk** 14(5):43-51.
- Ladyzhenskaya, O.A. (1963). Mathematical analysis of Navier-Stokes equation of incompressible liquids. **Annual Review of Fluid Mechanics** 7:249-272.
- Miranda, A.I.P., Oliveira, P.J., and Pinho, F.T. (2008). Steady and unsteady laminar flows of Newtonian and generalized Newtonian fluids in a planar T-junction. **International Journal for Numerical Methods in Fluids** 57:295-328.
- Moshkin, N.P. (1983). Numerical simulation of viscous incompressible flow in channel under preassigned pressure overfall. **Trudy IX Vsesouznoi Shkoly Sem-**

inara, **Institute of Theoretical and Applied Mechanics, Novosibirsk**
50-54.

Moshkin, N.P. (1985). Method for solution of flowing problem on the "stream function, curl" variable. **Numerical Methods for Continuum Mechanics** 15(3):120-127.

Moshkin, N.P. (1986). Numerical simulation of non-stationary viscous fluid flow with reassigned pressure drops. **The IV International Conference on Boundary and Interior Layers (BAIL-IV)**. Abstracts, Novosibirsk.

Moshkin, N.P., and Mounnamprang, P. (2003). Numerical simulation of vortical ideal fluid flow through curved channel. **International Journal for Numerical Methods in Fluids** 41:1173-1189.

Muzaferija, S. (1994). **Adaptive Finite Volume Method for Flow Predictions Using Unstructured Meshes and Multigrid Approach**. Ph.D. thesis, University of London.

Patankar, S.V. (1980). **Numerical Heat Transfer and Fluid Flow**. Hemisphere, New York.

Popiel, C.O., and Wojtkowiak J. (2000). Friction Factor in U-type undulated pipe flow. **Journal of Fluids Engineering** 122:260-263.

Ragulin, V.V. (1976), On the problem of viscous fluid flow through bounded domain with given pressure or force. **Dinamika Sploshn. Sredy, Novosibirsk** 27:78-92.

Ragulin, V.V., and Smagulov, S.h. (1980). On the smoothness of solution in some boundary value problem for Navier-Stokes equation. **Chislennye Metody Mekhaniki Sploshn. Sredy, Novosibirsk** 11(4):113-121.

- Samarskij, A.A., and Nikolaev, E.S. (1989). **Numerical Methods for Grid Equations**. Birkhauser Verlag Basel.
- Sheu, T.W.H., Tsai, S.F., Hwang, W.S., and Chang, T.M. (1999). A finite element study of blood flow in total cavopulmonary connection. **Computer & Fluids** 28:19-39.
- Temam, R. (1981). **Navier-Stokes equation: Theory and Numerical Analysis**. American Mathematical Society.
- Tsui, Y.Y., and Lu, C.Y. (2006). A study of the recirculating flow in planar, symmetrical branching channels. **International Journal for Numerical Methods in Fluids** 50:235-253.
- Warsi, Z.U.A. (1993). **Fluid Dynamics, Theoretical and Computational Approaches**. CRC Press, New York.
- William, L.B., and Graham, F.C. (2007). On a boundary condition for pressure-driven laminar flow of incompressible fluids, **International Journal for Numerical Methods in Fluids** 54:313-325.

APPENDICES

APPENDIX A

EXACT SOLUTIONS

A.1 Analytical solution of steady flow between two parallel plates

Let the flow between two parallel plates is considered. The upper plate is $y = h$ and the lower plate $y = 0$. The simplest problem of viscous fluid motion

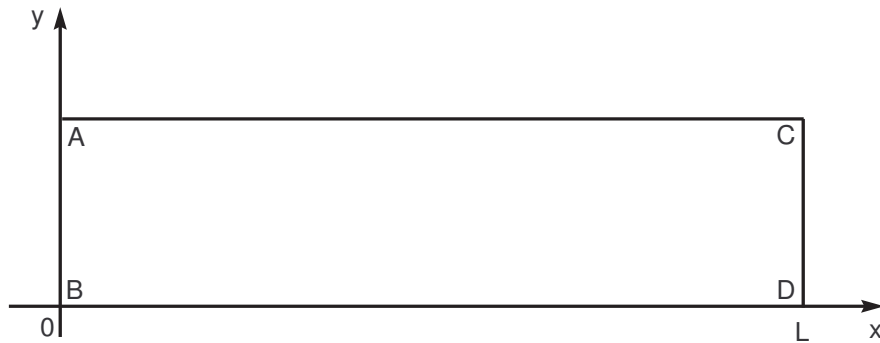


Figure A.1 Sketch of problem domain

is the flow between two parallel plates, the flow takes place along the x -axis under the action of a pressure is function of x . If x is the direction of main flow then $u_x = v \neq 0, u_y = u_z = 0$. The continuity is then simply

$$\frac{\partial v}{\partial x} = 0,$$

then we conclude that $v = v(y)$. The equations of motion reduce to one equation which is

$$\nu \frac{\partial^2 v}{\partial y^2} = \frac{1}{\rho} \frac{\partial p}{\partial x}, \quad \frac{\partial p}{\partial x} = \text{const}, \quad (\text{A.1})$$

where ν is the kinematics viscosity and ρ is the density. The no-slip boundary conditions

$$v(y) = 0, \quad y = 0, y = h, \quad (\text{A.2})$$

specified on the upper and lower plates. The solution of boundary value problem (A.1) and (A.2) can be written as

$$v(y) = \frac{1}{2\mu} \frac{dp}{dx} y^2 + C_1 y + C_2$$

Applying the no-slip boundary conditions (A.2), we have

$$v(y) = \frac{1}{2\mu} \frac{dp}{dx} (y^2 - hy). \quad (\text{A.3})$$

The flux of fluid through a section normal to the x -axis is

$$Q = \int_0^h v \, dy = -\frac{h^3}{12\mu} \frac{dp}{dx},$$

and the average velocity over a section is

$$U_m = \frac{Q}{h} = -\frac{h^2}{12\mu} \frac{dp}{dx}. \quad (\text{A.4})$$

Then the center line velocity U_c is

$$U_c = v(y)_{y=\frac{h}{2}} = -\frac{h^2}{8\mu} \frac{dp}{dx}, \quad (\text{A.5})$$

and $U_m = 2U_c/3$. Integrating equation A.4 with respect to x , we have

$$p = -\frac{12\mu U_m}{h^2} x + p_0, \quad p_0 = \text{const}. \quad (\text{A.6})$$

The Darcy friction coefficient is defined as

$$f_w = \frac{\Delta p}{\frac{1}{2}\rho U_m^2 \frac{L}{h}}. \quad (\text{A.7})$$

where U_m is the average velocity, ρ is the density of the fluid, L is the length of two parallel plates, h is the width between upper and lower plates, and $\Delta p = p_0 - p_L$

is the pressure difference between through-flow part AB and CD . Using equation (A.6) then

$$\frac{\Delta p}{L} = -\frac{\partial p}{\partial x} = \frac{12\mu U_m}{h^2}. \quad (\text{A.8})$$

Substituting equation (A.8) in equation (A.7), we have

$$f_w = \frac{24}{Re_m}, \quad Re_m = \frac{U_m h}{\nu}. \quad (\text{A.9})$$

Since $U_m = \frac{2U_c}{3}$, we have

$$\lambda = \frac{36}{Re_c}, \quad Re_c = \frac{U_c h}{\nu}. \quad (\text{A.10})$$

A.2 Analytical solution of oscillating flow between two parallel plates

The analytical solution for oscillating laminar channel flow between two parallel plates is presented. The upper plate is $y = h$ and the lower plate $y = 0$. The flow is assumed to developed instantly leading to the following linear momentum equation

$$\begin{aligned} \frac{\partial v}{\partial t} - \nu \frac{\partial^2 v}{\partial y^2} &= -\frac{1}{\rho} \frac{\partial p}{\partial x}, \quad 0 \leq y \leq h, \\ p(0, t) - p(L, t) &= \Delta p \cos(\omega t), \end{aligned} \quad (\text{A.11})$$

The initial data at $t = 0$ is $v(y, 0) = 0$ and no-slip boundary conditions $v(0, t) = v(h, t) = 0$, specified on the upper and lower plates. The problem is dimensionalized with height of channel, h , as the length scale, $\Delta p h / L$ as the pressure scale, $\sqrt{\Delta p h} / \sqrt{\rho L}$ as the velocity scale, and $\sqrt{\rho h L} / \sqrt{\Delta p}$ as the time scale. So equation (A.11) in non-dimensional form problem is as follow

$$\begin{aligned} \frac{\partial v}{\partial t} - \frac{1}{Re_{\Delta p}} \frac{\partial^2 v}{\partial y^2} &= \cos(\eta t), \quad 0 \leq y \leq 1, \\ \eta &= \omega \sqrt{\frac{\Delta p}{\rho h L}}, \quad Re = \frac{h}{\nu} \sqrt{\frac{\Delta p h}{\rho L}}, \end{aligned} \quad (\text{A.12})$$

where η is non-dimensional frequency, and $Re_{\Delta p}$ is pressure Reynold number. Initial data at $t = 0$ is $v(y, 0) = 0$ with no-slip boundary conditions at the wall $v(0, t) = v(1, t) = 0$.

We shall assume that the desired solution $v(y, t)$ and the given function $f_n(t) = \cos(\eta t)$ can be expanded in term of the eigenfunctions $Y_n(y) = \sin(n\pi y)$ for each t , that is,

$$v_p(y, t) = \sum_{n=1}^{\infty} Y_n(y) T_n(t).$$

and

$$f(y, t) = \sum_{n=1}^{\infty} f_n(t) Y_n(y)$$

where

$$\begin{aligned} f_n(t) &= 2 \int_0^1 f(y, t) Y_n(y) dy \\ &= 2 \int_0^1 \cos(\eta t) \sin(n\pi y) dy \\ &= \frac{2[1 - \cos(n\pi)]}{n\pi} [\cos(\eta t)]. \end{aligned}$$

Because the $\sin(n\pi y)$ are orthogonal, this can be the case only it for $n = 1, 2, \dots$,

$$T_n(t) = \int_0^t e^{-\lambda_n^2(t-\tau)} f_n(\tau) d\tau, \quad \lambda_n = \frac{n\pi}{\sqrt{Re}}.$$

The solution for problem (A.12) with initial data $v(y, 0) = 0$, and no-slip boundary conditions $v(y, t) = 0, y = 0, y = 1$. is

$$\begin{aligned} v(y, t) &= \sum_{n=1}^{\infty} \left\{ b_n \sin(n\pi y) \int_0^t e^{-\lambda_n^2(t-\tau)} \cos(\eta\tau) d\tau \right\}, \\ \lambda_n &= \frac{n\pi}{\sqrt{Re}}, \quad b_n = \frac{2[1 - \cos(n\pi)]}{n\pi}, \quad n = 1, 2, \dots \end{aligned} \tag{A.13}$$

CURRICULUM VITAE

NAME: Damrongsak Yambangwai. **GENDER:** Male. **NATIONALITY:** Thai.

DATE OF BIRTH: April 28, 1978. **MARITAL STATUS:** Single.

EDUCATIONAL BACKGROUND:

- B.Sc. in Mathematics, Kasetsart University, Bangkok, Thailand, 1999.
- M.Sc. in Computational Science, Suranaree University of Technology, Nakhon Ratchasima, Thailand, 2002.

PUBLICATIONS:

- D. Yambangwai and S. Muangchan, "Parallel algorithm based on explicit and implicit splitting method for Laplace equation", The 8th Annual National Symposium on Computational Science and Engineering, 2004, Suranaree University of Technology, Nakhon Ratchasima, Thailand.
- D. Yambangwai and N.P. Moshkin, "Finite volume method for incompressible flow through problem driven by a pressure drop", The 10th Annual National Symposium on Computational Science and Engineering, 2006, Chiang Mai University, Chiang Mai, Thailand.
- D. Yambangwai and N.P. Moshkin, "Finite volume method for the prediction of incompressible flow through a bounded domain with specified pressure as a boundary", The 12th Annual National Symposium on Computational Science and Engineering, 2008, Ubon Rajathanee University, Ubon Rajathanee, Thailand.

SCHOLARSHIPS:

- Development and Promotion of Science and Technology Talents Project (DPST), 1996-2004.
- The Royal Golden Jubilee Ph.D. Program (RGJ), 2005-2008.